Microtubule regulation of integrin-based adhesions is mediated by myosin-IIA

Yukako Nishimura*[1], Nisha Bte Mohd Rafiq*[1,3], Sergey V. Plotnikov[2], Zhen Zhang[1], Visalatchi Thiagarajan[1], Meenubharathi Natarajan[1], Gareth E. Jones[3], Pakorn Kanchanawong[1,4] and Alexander D. Bershadsky[1,5]

*Equal contributions

[1]Mechanobiology Institute, National University of Singapore, Singapore 117411, Singapore
[2]Department of Cell and Systems Biology, University of Toronto, Toronto, Ontario, Canada M5S 3G5
[3]Randall Division of Cell & Molecular Biophysics, King's College London, London SE1 1UL, UK
[4]Deparment of Biomedical Engineering, National University of Singapore, Singapore 117411
[5]Department of Molecular Cell Biology, Weizmann Institute of Science, Rehovot 76100, Israel

Keywords: actomyosin contractility, focal adhesions, GEF-H1, KANK, podosomes, SIM

Lead contact and correspondence to: alexander.bershadsky@weizmann.ac.il

Abstract

The role of microtubules in the mechanoregulation of integrin-mediated adhesions is poorly understood. Here, we show that uncoupling of microtubules from integrin adhesions by depletion or displacement of KANK family proteins connecting the adhesion protein talin with microtubule tips led to disruption of podosomes and augmentation of focal adhesions, similarly to total disruption of microtubules. Using structured-illumination microscopy, we demonstrate that microtubule uncoupling from adhesions or total microtubule disruption brings about a massive assembly of myosin-IIA filaments, whilst a burst of microtubule polymerization led to a transient disassembly of myosin-IIA filaments. We showed that myosin-IIA filaments are indispensable for microtubule-dependent regulation of focal adhesions and podosomes. The microtubule-driven control of myosin-IIA filament formation is achieved through the regulation of Rho by microtubule-localized Rho guanine nucleotide exchange factor GEF-H1. Thus, a unifying mechanism of microtubule-mediated regulation of focal adhesions and podosomes operates via KANKs- and GEF-H1-dependent local reorganization of myosin-II filaments.

Introduction

Crosstalk between microtubules and the actin cytoskeleton underlies many aspects of cell morphogenesis and migration. In particular, cell matrix adhesions that can be considered as peripheral domains of the actin cytoskeleton are well known to be controlled by the microtubule system in many cellular models. Microtubule-driven alterations in cell-matrix adhesions are thought to be responsible for many microtubule-mediated changes in cell shape, polarization and migration (Bouchet and Akhmanova, 2017; Kaverina and Straube, 2011; Linder et al., 2011; Small et al., 2002; Stehbens and Wittmann, 2012; Wittmann and Waterman-Storer, 2001). The molecular mechanisms of microtubule-dependent regulation of cell-matrix adhesions are however not fully understood.

Focal adhesions are elongated micron-sized clusters of transmembrane integrin molecules associated with a complex network of so-called plaque proteins that connect them to bundles of actin filaments (Geiger et al., 2009; Geiger and Yamada, 2011; Horton et al., 2016; Zaidel-Bar et al., 2007). Mature focal adhesions evolve from small nascent adhesions that form underneath the lamellipodia in a force-independent manner. However, for maturation into focal adhesions, application of mechanical force generated by actomyosin contractility and formation of actin bundles transmitting such forces are required (Bershadsky et al., 2006b; Gardel et al., 2010; Oakes and Gardel, 2014; Vicente-Manzanares and Horwitz, 2011; Vicente-Manzanares et al., 2009; Zaidel-Bar et al., 2015). It was shown long ago that disruption of microtubules by microtubule-depolymerizing agents leads to a substantial increase in the size and in some cases the number of mature focal adhesions (Bershadsky et al., 1996), whilst microtubule outgrowth following washout of microtubule-depolymerizing drugs leads to a transient decrease in size or even the disappearance of focal adhesions (Ezratty et al., 2005). In addition, growing microtubules are targeted to focal adhesions so that their plus ends form multiple transient contacts with these structures (Kaverina et al., 1998; Krylyshkina et al., 2002). Several mechanisms for such targeting have been suggested

(Ballestrem et al., 2004; Bershadsky et al., 2006b; Kaverina and Straube, 2011; Stehbens et al., 2014; Wu et al., 2008). In particular, recent studies, revealed that a novel component of focal adhesions, talin-binding proteins KANK1 and KANK2, can physically connect focal adhesions and microtubule tips via interaction with microtubule plus end-tracking proteins (Bouchet, 2016; Clohisey et al., 2014; Sun et al., 2016).

Podosomes represent another type of cell-matrix adhesion common in cells of monocytic origin but found also in cells of several other types (Cox and Jones, 2013; Kedziora et al., 2016; Murphy and Courtneidge, 2011). The characteristic structural feature of a podosome is an actin core perpendicular to the ventral cell membrane formed due to Arp2/3-dependent actin polymerization. The actin core is associated with an approximately ring-shaped cluster of adhesion proteins including transmembrane integrin molecules and the plaque molecules (paxillin, talin, vinculin etc.) connecting integrins to the actin network, essentially similar to those in focal adhesions. Importantly, in contrast to the case for focal adhesions, disruption of microtubules in macrophage-like cells is reported to result in a rapid disassembly of podosomes (Linder et al., 2000; Meddens et al., 2016).

Since the effects of microtubule disruption on focal adhesions and podosomes are reversed, one can suggest that microtubules regulate these integrin adhesions using different effectors. In our study reported here we surprisingly found a uniform mechanism underlying the effect of microtubules on both focal adhesions and podosomes. Firstly, we found that uncoupling of microtubules from focal adhesions and podosomes by interfering with KANK1 or KANK2 function faithfully reproduced the opposite effects of microtubule disruption on these two structures. Next, we found that in both cases the effectors are myosin-II filaments, which are strongly augmented upon uncoupling microtubules from the adhesion structures. Finally, such activation depends on the microtubule-associated RhoGEF, GEF-H1, which activates the Rho-ROCK signaling axis. Thus, KANK and GEF-H1-dependent local regulation of myosin-II filaments assembly appears to be a general mechanism

underlying the effects of microtubules on both classes of integrin-mediated adhesions.

Results

Disruption of microtubules or uncoupling them from integrin-based adhesions results in augmentation of focal adhesions and suppression of podosomes

We addressed the effect of perturbations of the microtubule network on two types of integrin-mediated adhesions of cells to extracellular matrix, focal adhesions and podosomes. Focal adhesions are characteristic of fibroblast-like cells and we chose to use the human fibrosarcoma cell line, HT1080, which has a well-developed system of focal adhesions associated with actin filament bundles known as stress fibers. For podosomes, we choose the human monocytic THP1 cell line, which upon treatment with transforming growth factor-beta 1 (TGFβ1) undergo differentiation into macrophage-like cells forming numerous podosomes. We used THP1 cells treated with TGFβ1 in all the experiments presented in this paper. These cells normally do not form stress fibers and focal adhesions but can be forced to do so by experimental manipulations such as inhibition of ARF1 (Rafiq et al., 2017).

To depolymerize microtubules in both cell types, we used 1 μM nocodazole. Such treatment disrupted the microtubules completely in less than 15 minutes in both cell types. To uncouple microtubules from adhesion structures in a more physiological manner, we employed recent findings that modular proteins of the KANK family (in particularly KANK1 and KANK2) physically connect microtubule tips with focal adhesions (Bouchet et al., 2016). Indeed, KANKs are known to interact with talin (a major integrin-associated protein localized to focal adhesions and podosome rings) and, via α and β liprins, with the membrane microtubule-targeting complex (ELKS, LL5β)(Bouchet et al., 2016), which in turn bind to CLASP end-tracking proteins (Lansbergen et al., 2006). In addition, KANK proteins can bind directly to the microtubule plus-end motor KIF21A (Bouchet et al., 2016; van der Vaart et al., 2013) and, at least in Drosophila, to EB1 (Clohisey et al., 2014). We then

compared the effects of total microtubule disruption with those caused by depletion of KANK1 or KANK2.

In agreement with previous studies, we found that disruption of microtubules led to an increase of focal adhesion number and size in HT1080 cells, but completely disrupted podosomes in TGFβ1-stimulated THP1 cells (Figure 1A,B, graphs G-I). Nocodazole washout led to recovery of podosomes (Supplementary Figure 1A-C, Movie S1). Of note, the disruption of microtubules and podosomes in THP1 cells by nocodazole was accompanied by formation of focal adhesion-like structures at the cell periphery (Figure 2, graphs G-I).

As shown by gene expression profiling (Supplementary Table 1), both KANK1 and KANK2 isoforms are expressed in the two cell lines used in this study, focal adhesion-forming HT1080 and podosome-forming THP1. Expression of two other isoforms, KANK3 and KANK4 was negligible. We confirmed previous observations on the localization of GFP-KANK1 and 2 around focal adhesion plaques (Bouchet et al., 2016; Sun et al., 2016) and demonstrated that in THP1 cells stimulated by TGFβ1, GFP-KANK1 and 2 also localize to the external ring surrounding podosomes (Figure 1E, Supplementary 2A and B).

Knockdown of KANK1 (Figure 1C) led to pronounced disruption of podosomes in TGFβ1-stimulated THP1 cells (Figure 1D, right panel, graphs H, I), phenocopying the effect of total microtubule disruption. Knockdown of KANK2 (Figure 1C) did not significantly affect podosome number in THP1 cells even though it increased the cell projection area (Figure 1 Graphs H, I, Supplementary Figure 2C-E). In HT1080 cells, knockdown of both KANK1 (Supplementary Figure 2F, graph G) and KANK2 (Figure 1D, left panel, graph G) produced an increase in focal adhesion size similar to total disruption of microtubules by nocodazole (Figure 1B, left panel). In our further experiments, we mainly focused on the role of KANK1 in THP1 cells and KANK2 in HT1080 cells.

In addition to KANK1/2 knockdown, we uncoupled microtubules from integrin adhesions by overexpression of KANK1/2 truncated constructs, GFP-KANK1-KN and GFP-KANK2-KN, which bind to talin but not to microtubules (Bouchet et al., 2016; Sun et al., 2016). We anticipated that these constructs could compete with endogenous KANK1 and 2 for binding to talin. Indeed, expression of either GFP-KANK1-KN or GFP-KANK2-KN in HT1080 cells resulted in localization of these constructs to focal adhesions and elimination of endogenous KANK2 from this location (Supplementary Figure 1G). Thus we concluded that overexpression of GFP-KANK1/2-KN disconnects the focal adhesions from microtubules and examined how such treatment will affect focal adhesions. In HT1080 cells, overexpression of GFP-KANK2-KN led to an increase in focal adhesion size (Figure 1F, left panel, graph G) to a similar degree to KANK2 knockdown or nocodazole treatment. Consistently, overexpression of full-length GFP-KANK2, which should enhance association of microtubules with focal adhesions, resulted in a significant decrease in focal adhesion area (Figure 1 graph G).

Along the same line of reasoning, we overexpressed GFP-KANK1-KN in THP1 cells and found that such treatment led to significant reduction in podosome number and de novo appearance of focal adhesion-like structures, resembling the effects of KANK1 knockdown or nocodazole treatment (Figure 1F, right panel, graphs H, I). Exogenous GFP-KANK1-KN was localized to the few residual podosomes and the newly formed focal adhesions in these cells.

To further investigate the mechanism of KANK1/2 effects, we performed rescue experiments on KANK1-depleted THP1 cells and KANK2-depleted HT1080 cells using various deletion mutants of KANK1 and KANK2, respectively (Supplementary Figure 3A). We found that constructs consisting of talin-binding domain alone (GFP-KANK1-KN, GFP-KANK2-KN), or constructs lacking a talin-binding domain (GFP-KANK1-CC-Cter, GFP-KANK2ΔKN), which cannot link talin-containing structures

with microtubules, did not rescue the effects of KANK1 knockdown on podosomes and KANK2 knockdown on focal adhesions (Figure 1 graphs G-I, Supplementary Figure 3 D, E, J and K). At the same time, the constructs (GFP-KANK1ΔANKR, GFP-KANK2 (1-670)) containing the talin-binding domain together with the coil-coiled liprin-binding domain (Bouchet et al., 2016; Sun et al., 2016; van der Vaart et al., 2013) rescued the effects of KANK1 and KANK2 knockdowns respectively, similarly to the full-length KANK1 or KANK2 (Figure 1 graphs G-I, Supplementary Figure 3B, C, H and I). Of note, the c-terminal region of KANK1 missing from GFP-KANK1ΔANKR, GFP-KANK2 (1-670), which is known to be involved in binding KIF21A kinesin (van der Vaart et al., 2013), appeared to be dispensable for the KANK effects on podosomes and focal adhesions (Supplementary Figure 3 F and L).
Altogether, our data strongly suggest that KANK1 and KANK2 knockdown produced their effect on podosomes and focal adhesions respectively, due to uncoupling of microtubules from these talin-containing adhesion structures.

Myosin-II filaments mediate the effect of microtubules on integrin-based adhesions

We next visualized myosin-II filaments by imaging either GFP-tagged myosin-II regulatory light chain (GFP-MRLC) or myosin-IIA heavy chain antibody by super-resolution structured illumination microscopy (SIM). We observed that disruption of microtubules resulted in massive formation of new myosin-II filaments. This effect was especially dramatic in THP1 cells, which normally contain only a rim of myosin-II filaments associated with circumferential actin bundles at the cell periphery (Figure 2A, Movie S2). Upon addition of nocodazole, a rapid disassembly of podosomes occurs in parallel with a drastic increase in the number of new myosin-II filaments (Figure 2A, left panel and graph on the right, Movie S2). Approximately 1 hour following nocodazole addition, the newly formed myosin II filaments aligned in registry forming well-developed myosin-II filament stacks (Figure 2A, 2E and Movie S2). This process was accompanied by formation of short actin filament bundles, some of which were associated with newly formed focal adhesion-like structures (Figure 2E). Even though HT1080 cells contained some

myosin-II filaments associated with stress fibers prior to nocodazole treatment (Figure 2B, Movie S3), the disruption of microtubules significantly increased the amount of myosin-II filaments as shown in Figure 2B. This increase, as in the case of THP1 cells, was accompanied by growth of focal adhesions.

To ascertain whether myosin-IIA filament assembly and disassembly are causal factors that account for the observed changes in focal adhesions and podosomes, we interfered with myosin-II filament formation by siRNA-mediated knockdown of myosin-IIA. Consistent with previous studies (Even-Ram et al., 2007; Vicente-Manzanares et al., 2007), we demonstrated that myosin IIA-depleted HT1080 cells essentially lack mature focal adhesions but contain small nascent adhesions at the cell periphery (Supplementary Figure 4A). The total area of such nascent adhesions per cell did not change significantly upon microtubule disruption (Supplementary Figure 4A, graph B). In THP1 cells lacking myosin-IIA, podosome appearance did not differ from that seen in control cells (Figure 2D, graphs G, H). However, these podosomes were insensitive to disruption of microtubules by nocodazole (Figure 2E, graphs G, H). Thus, we conclude that depletion of myosin-IIA filaments abolished the effect of microtubule disruption on both focal adhesions and podosomes.

Knockdown of KANK1 in THP1 cells also produced significant increase of the number of myosin-IIA filaments (Figure 2F). In contrast to control cells (Figure 2D, left panel), in which myosin-II filaments were located only at the periphery, in KANK1-depleted THP1 cells, myosin-IIA filaments formed organized structures associated with the bundles of actin filaments (Figure 2F). Many cells, similarly to nocodazole-treated cells, demonstrated formation of focal adhesions associated with these bundles (Figure 2F, graph I). In HT1080 cells, KANK2 knockdown resulted in significant increase in formation of myosin-II filaments and focal adhesion area (Supplementary Figure 4C).

Next, we assessed whether myosin-IIA depletion would interfere with the effects of KANK knockdown on podosomes and focal adhesions. We found that THP1 cells with double knockdowns of KANK1 and myosin-IIA demonstrated numerous

podosomes unlike the cells with knockdown of KANK1 alone (Figure 2F, graphs G, H). Consistently, myosin-IIA knockdown in HT1080 cells permitted the formation of only nascent adhesions, abolishing the difference in focal adhesion size between KANK2-positive and KANK2 knockdown cells (Supplementary Figure 4C). Thus, KANK-dependent modulation of both focal adhesions and podosomes is mediated via regulation of myosin-II filament assembly.

While disruption of microtubules resulted in augmentation of focal adhesions, microtubule outgrowth after nocodazole washout led to transient disassembly of focal adhesions (Ezratty et al., 2005). Accordingly, nocodazole washout in HT1080 cells led to a decrease in myosin-II filaments in the first minutes (Figure 3A and graph 3B, Movie S4). We also performed traction force microscopy to characterize the myosin-II driven contractility of HT1080 cells upon microtubule outgrowth. The traction forces exerted by cells on a substrate decreased upon microtubule recovery (Figure 3C, D, and Movie S5), consistent with the reduction of myosin-II filaments number (graph 3B) but 20 minutes following the washout returned to the control level. The drop and increase in traction forces preceded the decrease and increase in focal adhesion area, respectively (Figure 3C).

Finally, we checked whether microtubule outgrowth disrupted focal adhesions in KANK2 knockdown cells. We found that KANK2-depleted HT1080 cells still preserved focal adhesions visualized by mTFP-vinculin during microtubule outgrowth (Figure 3E and F, Movie S6). Accordingly, these cells preserved higher levels of myosin-II filaments than control cells (Figure 3E, middle row, and F). These data suggest that microtubule outgrowth affects focal adhesions and myosin-II filaments only if microtubules can interact with focal adhesions locally via KANK.

Microtubules regulate myosin-II filament assembly via modulation of the Rho-ROCK signaling axis

Since the major pathway regulating myosin-II filament assembly is phosphorylation of the myosin-II regulatory light chain (Vicente-Manzanares et al., 2009), we examined how changes of activity of the upstream regulators of such phosphorylation, namely Rho kinase (ROCK) and its activator RhoA, affected the processes of microtubule-driven regulation of focal adhesions and podosomes. Microtubule disruption in THP1 and HT1080 cells resulted in an increase in the fraction of RhoA-GTP while outgrowth of microtubules after nocodazole washout led to a decrease of RhoA-GTP levels in both THP1 and HT1080 cells (Supplementary Figure 5A). KANK1 and KANK2 knockdown in HT1080 cells also led to increased RhoA-GTP levels (Supplementary Figure 5B, left panel). Consistent with the fact that only knockdown of KANK1 but not of KANK2 led to disruption of podosomes in THP1 cells, we found that KANK1 knockdown but not KANK2 knockdown led to an increase in RhoA-GTP levels in THP1 cells (Supplementary Figure 5B, right panel).

We further investigated how pharmacological inhibition or activation of the Rho/ROCK pathway affected the processes of podosome disruption upon microtubule depolymerization and focal adhesion disruption upon microtubule outgrowth. We found that Rho activation by the small peptide CN03, mimicked the disruptive effect of microtubule disassembly or KANK1 depletion on podosomes (Figure 4A, graphs G and H, Movie S7). Addition of DMSO or Y-27632 did not affect podosome formation in control THP1 cells (Figure 4B, C, graphs G and H, Movie S8 and S9). At the same time, inhibition of ROCK by Y-27632 was sufficient to prevent the podosome disruption normally seen after nocodazole treatment (Figure 4D, graphs G and H, Movie S10). Moreover, addition of Y-27632 to cells incubated with nocodazole for several hours and completely lacking podosomes, still efficiently rescued podosomes by disassembling myosin-II filaments within 5-10 minutes (Figure 4E, graphs G and H, Movie S11). Inhibition of ROCK by Y-27632 led also to

rescue of podosomes in KANK1 knockdown THP1 cells (Figure 4F, graphs G and H, Movie S12). Of note in this experiment, the delay between myosin-II filament disruption and appearance of podosomes was as long as 30 minutes to 1 hour. In HT1080 cells, expression of either constitutively active RhoA (Q63L), or constitutively active ROCK mutant (rat Rok-alpha 1-543aa) prevented the disruptive effect of microtubule outgrowth on focal adhesions (Figure 4I, graphs J and K, Movie S13). Thus we conclude that microtubules regulate focal adhesions and podosomes through a single pathway modulating the level of Rho/ROCK activity.

RhoGEF GEF-H1 is a major mediator of the microtubule effect on myosin-II filaments, focal adhesions and podosomes

The major Rho nucleotide exchange factor associated with microtubules in mammalian cells is GEF-H1 (Krendel et al., 2002). We investigated the effects of GEF-H1 depletion on the effects of microtubule disruption or KANK1 and KANK2 knockdowns on the integrity of focal adhesions and podosomes as well as assembly of myosin-II filaments in THP1 and HT1080 cells. GEF-H1 knockdown THP1 cells (Figure 5A) essentially preserved the phenotype of control cells, having myosin-II filaments at the periphery and podosomes occupying the central part of the cells (Figure 5B and Supplementary Figure 6A). The integrity of the microtubule network was also unchanged in such cells (Supplementary Figure 6A). Nocodazole-induced disruption of microtubules in GEF-H1 knockdown cells was as efficient as in control cells but significantly did not lead to podosome disassembly (Figure 5 graphs E and F, Supplementary Figure 6B). Accordingly, microtubule disruption in GEF-H1 knockdown cells did not result in augmentation of myosin-II filaments and actin bundles associated with focal adhesions (Figure 5C, graph G, Supplementary Figure 6B). Moreover, double knockdown of GEF-H1 and KANK1 (Figure 5A) also did not lead to a reduction in podosome number, unlike the knockdown of KANK1 alone (Figure 5D, graphs E and F, Supplementary Figure 6C). Remarkably, GEF-H1 knockdown also prevented the effect of overexpression of KANK1 talin-binding domain, GFP-KANK1-KN. While GFP-KANK1-KN overexpression alone led to

significant disruption of podosomes and formation of focal adhesion-like structures (Figure 1F, right panel and Figure 5E, graphs F-H), the number of podosomes in GEF-H1 knockdown cells overexpressing GFP-KANK1-KN was similar to that in control cells and focal adhesions were completely absent (Figure 5E, graphs F-H).

In HT1080 cells lacking GEF-H1, the disruption of microtubules by nocodazole did not produce any increase of focal adhesion size (Supplementary Figure 7A and B, graph F and J). Similarly, double knockdown of KANK2 and GEF-H1 (Supplementary Figure 7G) did not increase focal adhesion size above its level in cells with knockdown of GEF-H1 alone (Supplementary Figure 7C and graph F). Similarly, knockdown of GEF-H1 reduced also the increase of focal adhesion size in cells overexpressing the talin-binding domain of KANK2, GFP-KANK2-KN (Supplementary Figure 7D and E, graph F). Of note, the focal adhesion size in cells lacking GEF-H1 was larger than that in control cells.

While in control HT1080 cells, microtubule outgrowth produced transient disassembly of focal adhesions (see above Figure 3A and B), in GEF-H1-depleted HT1080 cells, focal adhesion disruption by growing microtubules was less pronounced (Supplementary Figure 7H and I and graph F and J, Movie S14). Thus, the depletion of GEF-H1 significantly decreases the effects of microtubules on both podosomes and focal adhesions.

Discussion

In this study, we found a unifying mechanism for the microtubule-mediated regulation of focal adhesions and podosomes operating via KANKs- and GEF-H1-dependent local reorganization of myosin II filaments (Figure 6). It was previously shown that microtubule disruption induced disassembly of podosomes (Linder et al., 2000) but augmentation of focal adhesions (Bershadsky et al., 1996; Kaverina et al., 1998). Here, we show that these apparently opposite effects on the two integrin mediated adhesion systems can be reproduced by uncoupling of microtubules from integrin-based adhesions via knockdown of KANK family proteins which were shown to connect talin with protein complex trapping the microtubule plus ends (Bouchet et al., 2016). We found that KANK1 but not KANK2 knockdown mimics the effect of microtubule disruption on podosomes in THP1 cells. In fibroblasts, we focused on functions of KANK2 and found that its depletion increases, while its overexpression decreases, focal adhesion size similarly to microtubule disruption and outgrowth, respectively.

The effect of KANK1 or KANK2 knockdown can be mimicked by overexpression of KANK1 or KANK2 talin-binding domains lacking microtubule-binding domains, because of displacement of endogenous KANKs from the adhesion structures and the consequent uncoupling of microtubules from focal adhesions or podosomes. Consistent with this, the effects of KANK knockdowns can be abolished by KANK constructs that do connect microtubules with talin but not by constructs that can bind either to microtubules or talin alone. Thus, either disruption of microtubules or uncoupling them from integrin-based adhesions by knockdown or displacement of KANK proteins led to growth of focal adhesions and disruption of podosomes. KANK family proteins are probably not the only regulators of interaction of integrin-mediated adhesions with microtubules. In particular, the microtubule end-tracking protein CLASP1, was shown to interact with LL5β which can be associated with focal adhesions (van der Vaart et al., 2013). Interestingly, in data that supports our findings, knockdown of CLASP1 and CLASP2 led to stabilization of focal adhesions in

fibroblasts (Stehbens et al., 2014) and destabilization of podosomes in PDBu-stimulated vascular smooth muscle cells (Zhu et al., 2016).

Studying the effects of microtubule disruption or uncoupling from integrin adhesions using SIM microscopy, we were able to demonstrate that the major consequence of such treatments is a dramatic increase in the amount of myosin-II filaments. On the contrary, a burst of microtubule polymerization resulted in a transient decrease in the amount of myosin-II filaments. Using pharmacological and genetic manipulations affecting myosin-IIA filament assembly, we also showed that the dynamic changes in myosin-II filament assembly mediate both the disruptive and the stimulating effects of microtubules on podosomes and focal adhesions.

In light of these data, two questions deserve special discussion: (i) how microtubule disruption or uncoupling from the adhesion structures can affect myosin-II filament assembly and, (ii) why does the increase in myosin-II filaments promote the growth of focal adhesions but induce disassembly of podosomes?

To address the first question, we investigated whether the RhoGEF GEF-H1, known to be associated with microtubules (Krendel et al., 2002; Kwan and Kirschner, 2005; Ren et al., 1998), was involved in microtubule-dependent regulation of myosin-II filament formation. We have shown that knockdown of GEF-H1 renders the level of myosin-II filament polymerization independent of microtubule integrity or their association with adhesion structures. Accordingly, in GEF-H1 knockdown cells, neither microtubule disruption nor KANKs depletion led to podosome disassembly or focal adhesion growth. It is well recognized that GEF-H1-dependent activation of myosin-II filament assembly is mediated through activation of Rho and Rho kinase (Chang et al., 2008). Indeed, in our experiments the activation of Rho in THP1 cells by the Rho activator CN03 produced the same effects on focal adhesions and podosomes as disruption of microtubules or KANK knockdown. In further support of this idea, the lack of effect of KANK2 knockdown on podosomes in THP1 cells is consistent with the fact that such knockdown did not increase RhoA-GTP levels.

One caveat remains to be addressed. Our data do not fit the simple hypothesis of GEF-H1 regulation by microtubules (Birkenfeld et al., 2008), according to which GEF-H1 is inactive when associated with microtubules and undergoes activation upon release from the microtubules as a result of microtubule disruption. Our experiments in contrast showed that GEF-H1 could be activated after KANK knockdown or overexpression of KANK talin binding domain (KN) in a situation where microtubule integrity was preserved. These data open an interesting possibility that uncoupling of microtubules from integrin-mediated adhesions led to activation of GEF-H1, while targeting of the microtubules to the adhesions promotes its inactivation. Previous studies already demonstrated that knockdown of KANK1 (Kakinuma et al., 2008) and KANK2 (Gee et al., 2015) led to activation of Rho. These studies did not reveal the role of GEF-H1 in such activation. Our experiments showed that not only KANK1 depletion but just its uncoupling from talin by overexpression of KANK1-KN increased active Rho level (monitored by visualization of myosin-II filaments) in a GEF-H1-dependent fashion. Moreover, the KANK constructs lacking microtubule-binding domains cannot reduce the Rho level and rescue the podosomes in THP1 cells lacking KANK1. Altogether, these data suggest that not just the presence of KANK in the cytoplasm but its simultaneous link to talin and microtubules is needed for suppression of Rho activity most probably by inhibition of GEF-H1. The data by Kakinuma et al. (2008) on involvement of KANK interaction with 14-3-3 protein complex in KANK-dependent inhibition of Rho provide a clue to a possible mechanism of such regulation. 14-3-3 is known to interact with the cytoplasmic domain of integrins (Bonet et al., 2013) and form a ternary complex with integrin and talin (Chatterjee et al., 2016). At the same time, 14-3-3 was shown to inhibit GEF-H1 activity (Meiri et al., 2014; Zenke et al., 2004). Thus, under conditions where microtubules are associated with integrin adhesions, KANK could inhibit GEF-H1 by transferring 14-3-3 from integrin to microtubule tips where inactivation of GEF-H1 can occur. This hypothesis may explain why a link between microtubules and talin-containing adhesion complexes is needed for the Rho inactivation. Finally, we cannot exclude that vimentin intermediate filaments,

depletion of which is known to activate GEF-H1 (Jiu et al., 2017) may also contribute to this regulation.

A complex crosstalk between microtubules, Rho, myosin-II, and cell-matrix adhesions obviously involves many regulatory elements. In particular, effects of microtubules on focal adhesions were attributed to functions of kinesin-1 (Krylyshkina et al., 2002; Rodionov et al., 1993), Eg5 kinesin (Even-Ram et al., 2007), MYPT1 and HDAC6 (Joo and Yamada, 2014), FAK and dynamin (Ezratty et al., 2009; Ezratty et al., 2005) and APC (Juanes et al., 2017), while effects on podosomes are thought to involve kinesin KIF1C (Efimova et al., 2014; Kopp et al., 2006), kinesin KIF9 (Cornfine et al., 2011), and CLASPs (Efimova et al., 2014; Zhu et al., 2016). The role of microtubule-associated RhoGAPs such as ARHGAP18 cannot also be excluded (Lovelace et al., 2017). Unraveling this complex network and modes of GEF-H1 regulation is a subject for future studies.

The key findings of this study – that apparently opposite effects of microtubules on focal adhesions and podosomes is mediated by the same mechanism, namely, modulation of the assembly/disassembly of myosin-IIA filaments – left open the question of why the myosin-II filaments affect podosomes and focal adhesions in such a different manner. The relationship between myosin-II filaments and focal adhesions has been discussed often in the literature (Bershadsky et al., 2003; Gardel et al., 2010; Geiger et al., 2009; Oakes and Gardel, 2014; Vicente-Manzanares et al., 2009). The traction force generated by myosin-II filaments promotes assembly of mechanosensitive focal adhesions (Bershadsky et al., 2006a; Riveline et al., 2001). Indeed, in our study, the decrease of traction forces preceded the disassembly of focal adhesions induced by microtubule outgrowth, while increase of traction forces preceded the re-assembly of focal adhesion. In addition, myosin-II filaments stabilize the stress fibers associated with the focal adhesions, which can also promote an increase in focal adhesion size (Choi et al., 2008; Oakes et al., 2012). In the case of podosomes, myosin-IIA filaments were detected at the rim of podosomes and are reported to participate in the regulation of their dynamics (Dries et al.,

2013; Labernadie et al., 2014; Meddens et al., 2016), sometimes reducing podosome size and protrusion (Dries et al., 2013). The organization of the actin core of podosomes differs from the organization of actin plaques of focal adhesions and their associated actin bundles. It is essentially based on WASP-Arp2/3-mediated branched (dendritic) network of actin filaments, similar to that seen in lamellipodial protrusions where WAVE substitutes for WASP (Murphy and Courtneidge, 2011; Schachtner et al., 2013). It is possible that such a dendritic F-actin organization is incompatible with the presence of excess myosin-II filaments and thus undergoes rapid transformation into actomyosin bundle-like structures instead. Another hypothesis is based on the fact that existence of podosomes depends on generation of membrane curvature by podosome components interacting with the membrane such as dynamin and FBP17. Submembranous myosin-II filaments on the contrary appear to reduce membrane curvature (Elliott et al., 2015; Fischer et al., 2009) and therefore could antagonize podosome integrity. The mechanism of antagonistic relationship between myosin-II filaments and podosomes will hopefully be elucidated in future studies.

The mechanism of myosin-II dependent regulation of integrin-mediated adhesions by microtubules reported in this study can work in the processes of cell polarization and directional migration. Microtubules at the leading edge of the cell may reduce contractility and prevent formation of large focal adhesions facilitating extension of lamellipodia (Kaverina et al., 2000). In podosome-forming cells, microtubule-driven suppression of myosin-II activity can promote formation of podosomes towards the leading edge, which may enhance directional cell movement (Jones et al., 2002). In addition, at the trailing edge of the cell, effects of microtubules on myosin-II contractility and focal adhesions could promote tail retraction (Ballestrem et al., 2001; Rid et al., 2005; Sun et al., 2016).

Elucidation of the mechanisms underlying the effect of microtubules on integrin-mediated adhesions might be important for understanding and preventing the pathological migration of cells in the processes of metastasis. It is becoming

increasingly clear that known anti-cancer effects of the drugs affecting microtubules cannot be entirely explained only in terms of inhibition of mitosis (Bates and Eastman, 2017; Florian and Mitchison, 2016). There are many examples showing that such inhibitors affect either migration of tumor cells themselves or tumor-associated angiogenesis processes (Field et al., 2014). The understanding that myosin-II filaments are universal effectors that mediate the microtubule-driven regulation of adhesion structures sheds a new light on the mechanism of action of these inhibitors and suggest possible new strategies for the development of druggable targets and new treatments.

In conclusion (Figure 6), we demonstrated that uncoupling of microtubules from integrin-mediated adhesions results in profound re-organization of these structures. Myosin-II filaments operate as the universal effectors of microtubules in controlling integrin-based adhesions. Microtubule-dependent regulation of myosin-II filaments is mediated by GEF-H1, whose activity in turn depends upon microtubule association with integrin adhesions. This mechanism consists of an interwoven mix of signaling and mechanical events. Detailed elucidation of the particular elements of this fundamental regulatory network controlling cell to matrix adhesions will require further investigation.

Acknowledgements

We thank Anna Akhmanova (Utrecht University, Netherlands) and Reinhard Fäasler (Max Plank Institute for Biochemistry, Martinsried, Germany) for KANK1 and KANK2 constructs, respectively. We are grateful to Anna Akhmanova for useful discussions and constructive criticism. This research is supported by the National Research Foundation, Prime Minister's Office, Singapore and the Ministry of Education under the Research Centres of Excellence programme (A.D.B, N.B.M.R., T.V., and N.M.) and Singapore Ministry of Education Academic Research Fund Tier 3 (A.D.B, Y.N.) MOE Grant No. MOE2016-T3-1-002). N.B.M.R is also funded by a joint National University of Singapore-King's College London graduate studentship. G.E.J. is supported by the Medical Research Council, UK (G1100041, MR/K015664) and the generous provision of a visiting professorship from the Mechanobiology Institute, Singapore. P.K. and Z.Z. are funded by the Ministry of Education Academic Research Fund Tier 2 (MOE-T2-1-124), the Mechanobiology Institute seed funding, the National Research Foundation Fellowship (NRF-NRFF-2011-04), and the National Research Foundation Competitive Research Programme (NRF2012NRF-CRP001-084).

Author contributions

A.D.B. conceived and designed the project together with P.K. and G.E.J. Y.N. and N.B.M.R equally designed and performed all experiments and prepared the manuscript; Z.Z., T.V. and N.M. provided assistance in carrying out experiments and discussed results. A.D.B., G.E.J. and P.K. discussed results and prepared the manuscript.

Conflict of interest statement

The authors declare no competing financial interest.

Materials and Methods

Cell culture and cell transfection procedures

THP1 human monocytic leukemia cell line was obtained from Health Protection Agency Culture Collections (Porton Down, Salisbury, UK) and cultured in Roswell Park Memorial Institute media (RPMI-1640) supplemented with 10% heat-inactivated FBS and 50 μg/ml 2-Mercaptoethanol (Sigma-Aldrich) at 37°C and 5% CO_2. The suspended THP-1 cells were differentiated into adherent macrophage-like cells with 1 ng/ml human recombinant cytokine TGFβ1 (R&D Systems) for 24 or 48 hours on fibronectin-coated glass substrates. No apparent difference between the phenotype of cells stimulated for 24 or 48 hours were detected. For the imaging samples, 35-mm ibidi (Cat. 81158) glass-bottomed dishes were coated with 1 μg/ml of fibronectin (Calbiochem, Merck Millipore) in phosphate buffered saline (PBS) for 1-2 hours at 37°C, washed with PBS twice, and immersed in complete medium prior to seeding of cells. HT1080 human fibrosarcoma cell line was obtained from American Type Culture Collection (Manassas, VA, USA) and cultured in MEM supplemented with 10% heat-inactivated FBS, Non-essential amino acid and Sodium Pyruvate (Sigma-Aldrich), in an incubator at 37°C and 5% CO_2.

Cells were transiently transfected prior to stimulation with the expression vectors plasmids using electroporation (Neon Transfection System, Life Technologies) in accordance to manufacturer's instructions. Specifically, two pulses of 1400V of 20 ms duration were used for THP1 cells and one pulse of 950V of 50 ms was used for HT1080 cells. For siRNA-mediated knockdown, THP1 cells were transfected at the following concentrations: 150nM for KANK1 siRNA (Dharmacon, ON-TARGETplus SMARTpool siRNA, catalogue no. L-012879-01-0005), 100nM for KANK2 siRNA (Dharmacon, ON-TARGETplus SMARTpool siRNA, catalogue no. L-027345-00-0005), 150nM for MYH9 siRNA (Dharmacon, ON-TARGETplus SMARTpool siRNA catalogue no. L-007668-00-0005), and 150nM for GEF-H1 siRNA (Dharmacon, ON-TARGETplus SMARTpool siRNA, catalogue no. L-009883-00-0005). For control experiments, cells were transfected with non-targeting pool siRNA (Dharmacon,

ON-TARGETplus, catalogue no. D-001810-10) at a concentration similar to gene-targeted siRNAs. HT1080 cells were transfected at the following concentrations: 25nM for KANK1, 25nM for KANK2 siRNA, 50nM for MYH9 siRNA and 50nM for GEF-H1 siRNA (Dharmacon, see above) using DharmaFECT 1 transfection reagent (Dharmacon, catalogue no. T-2001) following the manufacturer's protocols.

Plasmids

Expression vectors for fluorescent protein fusion constructs were kindly provided by several laboratories, as follows: EGFP-KANK1, EGFP-KANK1-KN, EGFP-KANK1ΔANKR and EGFP-KANK1 CC-Cter (Bouchet et al., 2016) from Dr. Anna Akhmanova (Utrecht University, Utrecht, The Netherlands); EGFP-KANK2, EGFP-KANK2-KN, EGFP-KANK2 (1-670) and EGFP-KANK2ΔKN (Sun et al., 2016), from Dr. Reinhard Fässler (Max Planck Institute of Biochemistry, Germany); GFP-Vinculin (Zamir et al 1999), mCherry-Vinculin, mTFP-vinculin, mApple-MAP4, GFP-paxillin and mApple-Paxillin (Kanchanawong et al 2010), from Dr. Michael W. Davidson (Florida State University, FL, USA); GFP-RhoAQ63L, from Dr. Clare M. Waterman (National Institutes of Health, USA); FLAG-ROKα1-543, from Dr. Ronen Zaidel-Bar (Mechanobiology Institute, Singapore); human GFP-Myosin regulatory light chain (MRLC), from Dr. Mark Dodding (King's College London, UK). RFP-Zyxin (Tee et al., 2015), mouse GFP-MRLC (Hu et al., 2017), mCherry-UtrCH (Burkel et al., 2007), RFP-Lifeact and GFP-β-actin (Rafiq et al., 2017) were described previously.

Live cell observations

Pharmacological treatments were performed using the following concentrations of inhibitors or activators: 1 μM for Nocodazole (Sigma-Aldrich), 30-100 μM for Y-27632 dihydrochloride (Sigma-Aldrich), and 1 μg/ml for Rho Activator II (CN03, Cytoskeleton). For THP1 cells, duration of the treatment with the inhibitors was 1 hour. In some cases, cells were pre-treated with one inhibitor for 30 min and then another inhibitor was added for additional 1 hour. For nocodazole-washout

experiments, transfected HT1080 cells were plated on collagen I- coated coverslips for overnight. One hour prior to imaging, nocodazole in fresh L-15 medium (Leibovitz, Sigma-Aldrich) with 10% FBS was added to the cells. The coverslips were mounted in a perfusion chamber (CM-B25-1, Chamlide CMB chamber). Nocodazole was washed-out by fresh L-15 medium with FBS just prior to the start of the acquisition.

Immunoblotting

Cells were lysed in RIPA buffer 48 hours after transfection and extracted proteins were separated by SDS-PAGE in 4-20% SDS-polyacrylamide gel (Thermo Fisher Scientific) and transferred to PVDF membranes (Bio-Rad) at 75V for 2 hours. Subsequently, the PVDF membranes were blocked for 1 hour with 5% non-fat milk (Bio-Rad) or bovine serum albumin (BSA, Sigma-Aldrich), then incubated overnight at 4°C with appropriate antibodies: anti-KANK1 (Bethyl Laboratories, catalogue no. A301-882A, dilution 1:1000); anti-KANK2 (Sigma-Aldrich, catalogue no. HPA015643, dilution 1:1000); Anti-non muscle myosin-IIA (Sigma-Aldrich, catalogue no. M8064, dilution 1:1000); anti-GEF-H1 (Cell Signaling Technology, catalogue no. 4145, dilution 1:1000); anti-α-tubulin (Sigma-Aldrich, catalogue no. T6199, dilution 1:3000); anti-GAPDH (Santa Cruz Biotechnology, Inc., catalogue no. sc-32233, dilution 1:3000); anti-RhoA (Santa Cruz Biotechnology, Inc., catalogue no sc-418, dilution 1:1000).

Subsequently, the PVDF membranes were washed 3 times (10 minutes each) and probed by incubation for 1 hour with the appropriate secondary antibodies conjugated with horseradish peroxidase (Bio-Rad). The membranes were then washed three times (15 minutes at room temperature each), developed using Pierce™ ECL western blotting substratum (Thermo Fisher Scientific) and imaged by a ChemiDoc imaging system (Bio-Rad).

RhoA activity assay

THP1 and HT1080 cells were lysed in RIPA buffer for five minutes on ice as described in Pan et al. (2010), then centrifuged at 15,000g for five minutes at 4°C. The supernatant was incubated with Glutathione-agarose beads coated with GST-tagged Rho-binding domain of Rhotekin (provided by Dr. Boon Chuan Low (National University of Singapore) at 4°C for 30 minutes. The beads were washed three times with chilled RIPA buffer before being boiled in Laemmli buffer. Pulled-down RhoA was immunoblotted using respective antibodies as described above, and normalized to total RhoA in the whole cell lysates.

Immunofluorescence Microscopy

HT1080 cells were pre-fixed for 3 min at 37°C using 0.3 % Glutaraldehyde and 0.2% TritonX-100 in PHEM buffer (60 mM PIPES, 27 mM HEPES, 10 mM EGTA, 8 mM $MgSO_4 \times 7H_2O$, pH 7.0), and then post-fixed for 15 min at 37°C using 4 % PFA (Sigma-Aldrich) in PHEM buffer. After fixation, free aldehyde groups were quenched with 5 mg/ml Sodium borohydride (Sigma-Aldrich) for 5 min, and cells were washed 3 times for 5 min in PBS and blocked for 30 min in blocking solution (2 % Bovine Serum Albumin in PBS, Sigma-Aldrich). THP1 Cells were fixed for 15 min with 3.7% PFA in PBS, washed twice in PBS, permeabilized for 10 minutes with 0.5% triton X-100 (Sigma-Aldrich) in PBS, and then washed twice again in PBS. For microtubule visualization, cells were fixed and simultaneously permeabilized for 15 min at 37°C in a mixture of 3% PFA–PBS, 0.25% Triton-X-100 and 0.2% glutaraldehyde in PBS, and then washed twice with PBS for 10 min. Before immunostaining, samples were quenched for 15 min on ice with 1 mg/ml sodium borohydride in cytoskeleton buffer (10 mM MES, 150 mM NaCl, 5 mM EGTA, 5 mM $MgCl_2$, 5 mM glucose, pH 6.1).

Fixed cells were blocked with 5% BSA or 5% FBS for 1 hour at room temperature or overnight at 4°C prior to incubation with the following primary antibodies: anti-tubulin (Sigma-Aldrich, catalogue no. T6199, dilution 1:300); anti-paxillin (BD catalogue no. 610569, dilution 1:200); anti-vinculin (Sigma-Aldrich, catalogue no. V9131, dilution 1:400); anti-KANK2 (Sigma-Aldrich, catalogue no. HPA015643,

dilution 1:200); anti-non muscle heavy chain of myosin-IIA (Sigma-Aldrich, catalogue no. M8064, dilution 1:800). Samples were washed with PBS three times and incubated with Alexa Fluor-conjugated secondary antibodies (Thermo Fisher Scientific) for 1 hour at room temperature, followed by three washes in PBS. F-actin was visualized by Alexa Fluor 488 Phalloidin (Thermo Fisher Scientific), Phalloidin-TRITC (Sigma-Aldrich) or Alexa Fluor 647 Phalloidin (Thermo Fisher Scientific).

Fluorescence Microscopy

For structured illumination microscopy, two types of equipment were used: 1) spinning-disc confocal microscopy (Roper Scientific) coupled with the Live SR module (York et al., 2013), Nikon Eclipse Ti-E inverted microscope with Perfect Focus System, controlled by MetaMorph software (Molecular device) supplemented with a 100x oil 1.45 NA CFI Plan Apo Lambda oil immersion objective and sCMOS camera (Prime 95B, Photometrics), 2) Nikon N-SIM microscope, based on a Nikon Ti-E inverted microscope with Perfect Focus System controlled by Nikon NIS-Elements AR software supplemented with a 100x oil immersion objective (1.40 NA, CFI Plan-ApochromatVC) and EMCCD camera (Andor Ixon DU-897). For Total Internal Reflection Fluorescence (TIRF) microscopy, samples were imaged using a Nikon Ti-E inverted microscope controlled by Nikon NIS-Elements AR software, supplemented with a 60x 1.49 NA, Apo TIRF oil immersion objective lens and sCMOS camera (Orca Flash 4.0, Hamamatsu Photonics).

Traction Force Microscopy

Polyacrylamide gel substrates were prepared as previously described (Dembo and Wang, 1999). In brief, 25 mm round coverslips were activated by treatment with 1.2% 3-(Methacryloyloxy)propyltrimethoxysilane (Shin-Etsu Silicon, KBE-503) in 100 % methanol for 1h followed by extensive 100 % methanol washing. Then, freshly mixed solution of 0.145% bis/12% acrylamide with 100 nm yellow-green

fluorescent beads (FluoSpheres, 0.1µm, Thermo Fisher Scientific, Cat# F8803) was placed on dried- and activated- coverslips to give an adhered gel with stiffness of 16kPa. Coverslips with attached gel substrate were washed three times with 0.1M HEPES-NaOH buffer (pH 7.5) and conjugated with collagen I (Thermo Fisher Scientific, A1048301) using sulfo-SANPAH (Thermo Fisher Scientific) to facilitate cell attachment. HT1080 cells were plated on the polyacrylamide gel 2 hours prior to the experiment and images of focal adhesions by RFP-Zyxin and beads were acquired by spinning disk confocal microscope equipped with a 60X water immersion objective (NA1.2, UPlanApo, Nikon) as described above. After acquisition, 0.5 % trypsin-EDTA was added into chamber to remove all cells from the substrate, and then images of beads were captured again. The traction stress field was computed as described previously (Sabass et al., 2008).

Image processing and data analysis

The number of podosomes was quantified automatically by applying an ImageJ-based plugin for counting nuclei (ITCN) to images of the podosome core (F-actin). Quantification was validated by manual analysis of the first 5-10 cells in the specimen. The automated procedure usually detected more than 90% of the podosomes identified by manual counting. Line intensity profiles (arbitrary unit, a.u.) measuring the mean intensity of GFP or mCherry fluorescence per area (μm^2) by ImageJ Plugin, background-subtracted and normalized per maximal intensity in the field, yielding values ranging from 0 (lowest) to 1 (highest). For the morphometric analysis of focal adhesions in HT1080 cells, a custom-written software in IDL (Harris Geospatial Inc.) was used. Immunofluorescence images of paxillin were first background-subtracted using the rolling ball algorithm. Subsequently, focal adhesion region-of –interests (ROIs) were segmented using Otsu thresholding. The software determines the areas of individual focal adhesions. The total area of focal adhesion in ROIs was calculated by summing the value of individual focal adhesions. The focal adhesions of THP1 cells were labeled with

vinculin and measured using the same algorithm with RenyiEntropy or Otsu thresholding in ImageJ.

To analyze microtubules, fluorescence images of MAP4-labeled microtubules were used (Ganguly et al., 2013). The image processing was performed as described in Zhang et al. (2017). The enhanced images were then binarized to extract the microtubule traces by a threshold calculated using Otsu's method. For the analysis of myosin-II filaments (labeled by GFP-MRLC) and F-actin core in podosomes (labeled by mCherry-UtrCH), segmentation was performed by binarization using Otsu's threshold. The amounts of myosin-II, MAP4 and F-actin were computed as the total numbers of their segmented pixels.

Gene Expression profile

The transcriptomes of THP1 and HT1080 were mapped, quantified and indicated as fragments per Kilobase million (FPKM) using the RNA-Seq technology (Mortazavi et al., 2008). Briefly, the total RNA of THP1 and HT1080 cell lysates was extracted using the RNeasy Mini Kit (Qiagen) according to manufacturer's protocol. The extracted RNA was processed and analyzed by BGI Tech Solutions Co., Ltd.

Statistical analyses

Significance of the differences was calculated using two-tailed unpaired Student's *t*-test. The methods for statistical analysis and sizes of the samples (n) are specified in the results section or figure legends for all of the quantitative data. Differences were accepted as significant for $P < 0.05$. Prism version 6 (GraphPad Software) was used to plot, analyze and represent the data.

Figure legends

Figure 1

Disruption of microtubules or their uncoupling from adhesion structures by KANK knockdown or displacement suppressed podosome assembly but promoted focal adhesion formation. (A) Left panel: HT1080 cell transfected with control siRNA showed radially-organized microtubules (green) with numerous focal adhesions (red) at the cell periphery. Right panel: THP1 cells transfected with control siRNA and stimulated with TGFβ1 displayed radial microtubule organization (green) and numerous podosomes (red). (B) Addition of 1 μM nocodazole disrupted the microtubules (green) and induced formation of large focal adhesions in HT1080 cells (left panel, red) and disassembly of podosomes in THP1 cells (right panel, red).
(C) Western blots showing KANK1 and KANK2 levels in HT1080 cells (left panel) and TGFβ1-stimulated THP1 cells (right panel) transfected with scramble (control), KANK1 or KANK2 siRNAs; GAPDH and α-tubulin were used as a loading control.
(D) Knockdown of KANK2 in HT1080 cells (left panel) or KANK1 in THP1 cells (right panel) by siRNA did not interfere with microtubule integrity (green) but induced larger focal adhesions in HT1080 cells (left panel, red) and disassembly of podosomes in THP1 cells (right panel, red). Microtubules were visualized by immunostaining with α-tubulin antibody in both HT1080 and THP1 cells; focal adhesions were marked by expression of mApple-paxillin in HT1080 cells, while podosomes were visualized by TRITC phalloidin to label F-actin cores in THP1 cells.
(E) Left panel: GFP-KANK2 (green) was localized to the rim surrounding individual focal adhesions marked by paxillin (red). Right panel: GFP-KANK1 (green) was found to surround the actin cores of podosomes (red) in TGFβ1-stimulated THP1 cell. Boxed area selects two podosomes shown with high magnification in the insets (utmost bottom image, right image). (F) The HT1080 cell overexpressing the talin-binding domain of KANK2 (GFP-KANK2-KN, green) exhibited large focal adhesions (left panel, red) while THP1 cell overexpressing talin-binding domain of KANK1 (GFP-KANK1-KN, green) demonstrated reduced podosome number and formation

of focal adhesion-like structures (right panel, red). GFP-KANK2-KN (green) was localized to focal adhesions (red) in HT1080 cells (left panel), while GFP-KANK1-KN was localized to remaining podosomes in THP1 cells (right panel, red). In addition, KANK1-KN overlapped with short actin bundles indicating to putative focal adhesion-like structures as shown at high magnification in the inset corresponding to the boxed area (utmost bottom image, right panel). Focal adhesions were marked by expression of mApple-paxillin in HT1080 cells, while podosome actin cores and other F-actin structures were visualized by expression of mCherry-UtrCH in THP1 cells. (G) The area of individual focal adhesions (um^2) stained with anti-paxillin antibody in HT1080 cells and (H) the numbers of podosomes per cell visualized by phalloidin staining or mCherry UtrCH in THP1 cells are presented as box-and-whiskers plot (I) while the percentage of cells with more than 10 podosomes as mean ± SD. Nz=nocodazole. The significance of the difference between groups was estimated by two-tailed Student's *t*-test, the range of p-values >0.05(non-significant), ≤ 0.05, ≤0.01, ≤0.001, ≤ 0.0001 are denoted by "ns", one, two, three and four asterisks (*), respectively.

Figure 2

Myosin-II filaments mediate the effect of microtubules on integrin-based adhesions. (A and B) Addition of 1 μM nocodazole induced the assembly of numerous myosin-II filaments (green) in (A) THP1 and (B) HT1080 cells, which correlates with the disruption of podosomes (red) in THP1 cells (A) and increase in focal adhesion size (red) in HT1080 (B), respectively. Scale bars of each panel in (A) and (B) are 5 and 10 μm, respectively. Graphs on the right shows that upon microtubule disruption by nocodazole, the increase in the amount of myosin-II filaments was accompanied by both the decrease in podosome number in THP1 cell (A, upper row) and the increase in focal adhesion area in HT1080 cells (B, upper row). See also Movies S2 and S3 for both THP1 and HT1080 cells, respectively. Focal adhesions were marked by expression of mApple-paxillin in HT1080 cells, while podosome actin cores and other F-actin structures were visualized by expression of RFP-lifeact in THP1 cells.

Details of the quantification procedures can be found in the Materials and Method section. (C) Western blots showing KANK1 and myosin-IIA levels in TGFβ1-stimulated THP1 cells transfected with scramble (control), KANK1, or MYH9 siRNAs, as well as KANK1 and MYH9 siRNAs together. α-tubulin was used as a loading control. (D) Left panel: THP1 cells transfected with scrambled control siRNA showed circumferential assembly of myosin-II filaments (green) and numerous podosomes visualized by actin (red) and vinculin (purple) staining. Scale bars, 5μm. Boxed area shows higher magnification of small focal complexes and podosomes in the insets. Scale bars, 1μm. Right panel: Knockdown of MYH9 led to complete disappearance of myosin-IIA filaments but did not affect podosomes (actin: red; vinculin: purple). (E and F) Left panels: Microtubule disruption (E) or their uncoupling from podosomes by endogeneous KANK1 depletion (F) induced massive assembly and alignment of myosin-II filaments (green) as well as disruption of podosomes (red, purple) and formation of focal adhesion-like structures marked by vinculin (purple) staining. Scale bars, 5μm. Boxed area shows higher magnification of large focal adhesion-like structures in the insets. Scale bars, 1μm. Right panels: THP1 cells lacking myosin-IIA and treated with nocodazole (E) or with double knockdown of myosin-IIA and KANK1 (F) preserved the podosomes and do not form focal adhesions (actin:red; vinculin: purple). Scale bars, 5μm. (G-I) Quantification of the number of podosomes per cell (G), percentage of cells forming more than 10 podosomes (H) and area of focal adhesions (I) in THP1 cells treated as indicated in the previous figures (D-F). Nz=nocodazole. The significance of the difference between groups was estimated by two-tailed Student's *t*-test, the range of P-values >0.05(non-significant), ≤ 0.05, ≤0.01, ≤0.001, ≤ 0.0001 are denoted by "ns", one, two, three and four asterisks (*), respectively.

Figure 3

Augmentation of microtubule contacts with focal adhesions brings about disassembly of myosin-II filaments and focal adhesions. (A) Time-lapse observations of microtubules (upper row), segmented microtubules (second row) using open-

source software package called SIFNE (Zhang et al., 2017) and myosin-II filaments (bottom row) in the course of microtubule outgrowth after nocodazole washout in HT1080 cell. Time after the nocodazole washout is indicated in each frame. Microtubules and myosin-II filaments were labeled by mApple-MAP4 and GFP-MRLC, respectively. Note that recovery of microtubules is accompanied by disappearance of myosin-II filaments. See Movie S4. (B) Quantification of the changes in the amount of microtubules (blue) and myosin-II filaments (green) shown in (A). Details of the quantification procedures can be found in the Materials and Method section. (C) Changes in traction forces exerted by HT1080 cells in the course of microtubule recovery following nocodazole washout. The traction forces are presented in the upper row in spectrum scale (right). The corresponding images of cells with focal adhesions labeled with RFP-zyxin are presented in the bottom row, along with the time in minutes after nocodazole washout. Note that the traction forces and focal adhesion size began to decrease already in 1 minute following nocodazole washout but recover in about 20 minutes. See Movie S5. (D) Changes in sum of the absolute values of traction forces (kPa) and total focal adhesion area (μm^2) per cell shown in (C). Note that drop and subsequent increase of traction forces (red) preceded the drop and increase in focal adhesion area (blue), respectively. (E) KANK2 knockdown in HT1080 suppresses the effect of microtubule outgrowth on the amount of myosin-II filaments. Microtubules (upper row), segmented microtubules (second row), myosin-II filaments (bottom row) in the same cell were labeled as indicated in (A). Time after nocodazole washout is indicated in the upper row. See Movie S6. Note that in spite of microtubule outgrowth, the changes in myosin-II filaments were less pronounced than in control cell shown in (A). (F) Quantification of the changes in amount of microtubules (blue) and myosin-II filaments (green) was performed as in (B). (G) Changes in the total area of focal adhesions after nocodazole treatment and washout in control and KANK2 knockdown HT1080 cells. The cells before and after corresponding treatments were fixed and stained with paxillin antibody to visualize focal adhesions. Nz=nocodazole. Not less than 40 cells were measured for each type of

treatment. The data presented as box-and-whiskers plots and statistical significance of the difference (p-values) was calculated by two-tailed Student's *t*-test, the range of P-values >0.05(non-significant), ≤ 0.05, ≤0.01, ≤0.001, ≤ 0.0001 are denoted by "ns", one, two, three and four asterisks (*), respectively. Scale bars in all panels correspond to 10 μm.

Figure 4

Microtubules regulate myosin-II filaments, podosomes and focal adhesions via modulation of Rho-ROCK signaling axis. (A) Podosomes (red) and myosin-II filaments (green) in THP1 cell stimulated by TGFβ1 before (left two images) and after (right two images) addition of Rho activator, CN03. Note the assembly of new myosin-II filaments (green) and the disappearance of podosomes (red). See Movie S7. (B) THP1 cell stimulated with TGFβ1 before (left) and after (right) 1 hour incubation with DMSO. DMSO did not change the distribution of myosin-II filaments (green) and podosomes (red). See Movie S8. (C) THP1 cell stimulated with TGFβ1 before (left) and after (right) 1 hour incubation with Y-27632. Y-27632 eliminated the myosin-II filaments (green) but did not affect podosomes distribution (red). See Movie S9. (D) THP1 cell stimulated with TGFβ1 and pre-treated with Y-27632 for 30 minutes, shown before (left) and after (right) 1 hour incubation with nocodazole. Pre-treatment with Y-27632 prevented burst of myosin-II filaments typical for nocodazole treatment as well as the disruptive effect of nocodazole on podosomes (cf. Figure 2A). Podosomes are labeled in red; myosin-II filaments in green (absent in this cell). See Movie S10. (E) THP1 cell stimulated with TGFβ1 and pre-treated with nocodazole for 1 hour, shown before (left two images) and after (right two images) 1 hour incubation with Y-27632. Disassembly of myosin-II filaments (green) and recovery of podosomes (red) is seen in the right panel. See Movie S11. (F) KANK1-depleted THP1 cell shown before (left) and after (right) 1 hour incubation with Y-27632. Note the disappearance of myosin-II filaments (green) and recovery of podosomes (red) upon Y-27632 treatment. See Movie S12. Scale bars, 5 μm. (G and H) The number of podosomes (G) and the percentage of cells with more

than 10 podosomes (H) in THP1 cells treated as indicated in the previous figures (A-F). The significance of the difference between groups was determined as explained in Figure 1. (I-K) Constitutively active RhoA and ROCK1 prevented the disruption of focal adhesions upon microtubule outgrowth in HT1080 cells. Scale bars, 10 μm. (I) Time-lapse sequences showing focal adhesion dynamics after nocodazole washout in control (top row), cell expressing constitutive active RhoA-Q63L (middle row) and cell expressing dominant active ROCK (rat Rok-alpha 1-543aa). The focal adhesions were visualized by TIRF microscopy of cells expressing mApple-paxillin. Note that microtubule outgrowth after nocodazole washout led to disassembly of the focal adhesions while constitutively active RhoA and ROCK prevented this process. See Movie S13. (J) Intensities of mApple-paxillin fluorescence in focal adhesions normalized to the intensity level in the first frame, in control, RhoA-Q61L expressing and ROCK1-DA expressing cells shown in (I). (K) Total focal adhesion area in control cells and cells expressing RhoA-Q61L visualized in non-treated and nocodazole-treated for 1 hour cells and in cells fixed 30 minutes following nocodazole washout. Focal adhesions were visualized by paxillin antibody staining. Nz=nocodazole. Not less than 14 cells were measured for each type of treatment. The data presented as box-and-whiskers plots and statistical significance of the difference (p-values) was calculated by two-tailed Student's *t*-test, the range of P-values >0.05(non-significant), ≤ 0.05, ≤0.01, ≤0.001, ≤ 0.0001 are denoted by "ns", one, two, three and four asterisks (*), respectively.

Figure 5

GEF-H1 is required for the microtubule-driven regulation of the myosin-II filaments, focal adhesions and podosomes. (A) Western blot demonstrating siRNA-mediated depletion of GEF-H1, KANK1, and both of them in THP1 cells. α-tubulin is used as loading control. (B) Visualization of podosomes (actin: red, vinculin: purple) and myosin-II filaments (green) in cells from cultures transfected with control siRNA (left panel) and GEF-H1 siRNA (right panel). The distribution of both podosomes and myosin-II filaments were unchanged in GEF-H1 knockdown cell. (C) Effect of

microtubule disruption by on myosin-II filaments and podosomes in control (left panel) and GEF-H1 knockdown (right panel) cells. Labeling of myosin-II filaments and podosomes is the same as in (B). Note that increase in myosin-II filaments amount accompanied by disappearance of podosomes and appearance of vinculin-positive focal adhesions upon nocodazole treatment in control but not in GEF-H1 knockdown cells. (D) Podosomes, focal adhesions and myosin-II filaments in cells from KANK1 knockdown culture (left panel) and in cells from KANK1 and GEF-H1 knockdown culture. Labeling is the same as in (B) and (C). While KANK1 knockdown cell (left panel) demonstrate numerous myosin-II filaments and focal adhesions but not podosomes, the cells with KANK1/GEF-H1 double knockdown (right panel) preserved podosomes and did not show abundant myosin-II filaments. In (B-D), podosomes were visualized by phalloidin labeling of actin (red), and immunofluorescence staining of vinculin (purple). The myosin-II filaments in the same cells were labeled with MHCIIA antibody (green). (E) Disruption of podosomes by overexpression of GFP-KANK1-KN (left panel) is abolished in cells with knockdown of GEF-H1 (right panel). Actin was visualized by mCherry-UtrCH (red), GFP-KANK1-KN is shown in purple, and myosin-II filaments are shown in green. Scale bars for (B-E), 5 μm. (F-H) Quantification of the number of podosomes (F), percentage of cells forming more than 10 podosomes (G) and average area of focal adhesions (H) in control THP1 cells and cells treated as shown in the previous figures (B-D). Nz=nocodazole. Not less than 80 cells were assessed for each type of treatment. The statistical significance of the difference (p-values) was estimated by two-tailed Student's *t*-test.

Figure 6

A cartoon summarizing the results of the present study. (A) Microtubule coupled to integrin-containing adhesion structures via interaction of KANK family proteins with integrin-binding protein talin and the cortical microtubule docking site (CMDS, green), a complex of proteins (lipirins, ELKS, LL5β) trapping the microtubule plus end via interaction with EB1/CLASP proteins (Bouchet et al., 2016). The guanine

nucleotide exchange factor GEF-H1 is associated with peripheral segments of microtubules. Our findings suggest that coupling of microtubules to integrin adhesions via KANK proteins suppresses GEF-H1 activity. In such situations, the levels of Rho-GTP and activity of ROCK are low, and as a result only few myosin filaments are located in the proximity of adhesions. Such conditions are permissive for podosomes but limit the growth of focal adhesions. (B) and (C) Uncoupling of microtubule tips from integrin adhesions by either depletion of KANK (B) or displacement of endogenous KANK from talin by overexpression of the talin-binding KN domain of KANK (C) leads to activation of GEF-H1 and consequent activation of the Rho/ROCK signaling axis. As a result, the assembly of myosin-IIA filament stacks is significantly activated which is inimical to podosome existence. Myosin-II filaments remodel the actin cytoskeleton in the proximity of adhesions (actin filaments are not shown), favorable for the formation and growth of stress fiber-associated focal adhesions.

References

Ballestrem, C., Hinz, B., Imhof, B.A., and Wehrle-Haller, B. (2001). Marching at the front and dragging behind: differential alphaVbeta3-integrin turnover regulates focal adhesion behavior. The Journal of cell biology *155*, 1319-1332.

Ballestrem, C., Magid, N., Zonis, J., Shtutman, M., and Bershadsky, A. (2004). Interplay between the Actin Cytoskeleton, Focal Adhesions and Microtubules. In Cell Motility (John Wiley & Sons, Ltd), pp. 75-99.

Bates, D., and Eastman, A. (2017). Microtubule destabilising agents: far more than just antimitotic anticancer drugs. British journal of clinical pharmacology *83*, 255-268.

Bershadsky, A., Chausovsky, A., Becker, E., Lyubimova, A., and Geiger, B. (1996). Involvement of microtubules in the control of adhesion-dependent signal transduction. Current biology : CB *6*, 1279-1289.

Bershadsky, A., Kozlov, M., and Geiger, B. (2006a). Adhesion-mediated mechanosensitivity: a time to experiment, and a time to theorize. Curr Opin Cell Biol *18*, 472-481.

Bershadsky, A.D., Balaban, N.Q., and Geiger, B. (2003). Adhesion-dependent cell mechanosensitivity. Annual review of cell and developmental biology *19*, 677-695.

Bershadsky, A.D., Ballestrem, C., Carramusa, L., Zilberman, Y., Gilquin, B., Khochbin, S., Alexandrova, A.Y., Verkhovsky, A.B., Shemesh, T., and Kozlov, M.M. (2006b). Assembly and mechanosensory function of focal adhesions: experiments and models. European journal of cell biology *85*, 165-173.

Birkenfeld, J., Nalbant, P., Yoon, S.H., and Bokoch, G.M. (2008). Cellular functions of GEF-H1, a microtubule-regulated Rho-GEF: is altered GEF-H1 activity a crucial determinant of disease pathogenesis? Trends in cell biology *18*, 210-219.

Bonet, R., Vakonakis, I., and Campbell, I.D. (2013). Characterization of 14-3-3-zeta Interactions with integrin tails. Journal of molecular biology *425*, 3060-3072.

Bouchet (2016). Talin-KANK1 interaction controls the recruitment of cortical microtubule stabilizing complexes to focal adhesions. eLife.

Bouchet, B.P., and Akhmanova, A. (2017). Microtubules in 3D cell motility. Journal of cell science *130*, 39-50.

Bouchet, B.P., Gough, R.E., Ammon, Y.C., van de Willige, D., Post, H., Jacquemet, G., Altelaar, A.M., Heck, A.J., Goult, B.T., and Akhmanova, A. (2016). Talin-KANK1 interaction controls the recruitment of cortical microtubule stabilizing complexes to focal adhesions. eLife *5*.

Burkel, B.M., von Dassow, G., and Bement, W.M. (2007). Versatile fluorescent probes for actin filaments based on the actin-binding domain of utrophin. Cell motility and the cytoskeleton *64*, 822-832.

Chang, Y.C., Nalbant, P., Birkenfeld, J., Chang, Z.F., and Bokoch, G.M. (2008). GEF-H1 couples nocodazole-induced microtubule disassembly to cell contractility via RhoA. Molecular biology of the cell *19*, 2147-2153.

Chatterjee, D., Zhiping, L.L., Tan, S.M., and Bhattacharjya, S. (2016). Interaction Analyses of the Integrin beta2 Cytoplasmic Tail with the F3 FERM Domain of Talin

and 14-3-3zeta Reveal a Ternary Complex with Phosphorylated Tail. Journal of molecular biology *428*, 4129-4142.
Choi, C.K., Vicente-Manzanares, M., Zareno, J., Whitmore, L.A., Mogilner, A., and Horwitz, A.R. (2008). Actin and alpha-actinin orchestrate the assembly and maturation of nascent adhesions in a myosin II motor-independent manner. Nature cell biology *10*, 1039-1050.
Clohisey, S.M., Dzhindzhev, N.S., and Ohkura, H. (2014). Kank Is an EB1 interacting protein that localises to muscle-tendon attachment sites in Drosophila. PloS one *9*, e106112.
Cornfine, S., Himmel, M., Kopp, P., El Azzouzi, K., Wiesner, C., Kruger, M., Rudel, T., and Linder, S. (2011). The kinesin KIF9 and reggie/flotillin proteins regulate matrix degradation by macrophage podosomes. Molecular biology of the cell *22*, 202-215.
Cox, S., and Jones, G.E. (2013). Imaging cells at the nanoscale. The international journal of biochemistry & cell biology *45*, 1669-1678.
Dembo, M., and Wang, Y.L. (1999). Stresses at the cell-to-substrate interface during locomotion of fibroblasts. Biophysical journal *76*, 2307-2316.
Dries, K., Meddens, M.B., de Keijzer, S., Shekhar, S., Subramaniam, V., Figdor, C.G., and Cambi, A. (2013). Interplay between myosin IIA-mediated contractility and actin network integrity orchestrates podosome composition and oscillations. Nature communications *4*, 1412.
Efimova, N., Grimaldi, A., Bachmann, A., Frye, K., Zhu, X., Feoktistov, A., Straube, A., and Kaverina, I. (2014). Podosome-regulating kinesin KIF1C translocates to the cell periphery in a CLASP-dependent manner. Journal of cell science *127*, 5179-5188.
Elliott, H., Fischer, R.S., Myers, K.A., Desai, R.A., Gao, L., Chen, C.S., Adelstein, R.S., Waterman, C.M., and Danuser, G. (2015). Myosin II controls cellular branching morphogenesis and migration in three dimensions by minimizing cell-surface curvature. Nature cell biology *17*, 137-147.
Even-Ram, S., Doyle, A.D., Conti, M.A., Matsumoto, K., Adelstein, R.S., and Yamada, K.M. (2007). Myosin IIA regulates cell motility and actomyosin-microtubule crosstalk. Nature cell biology *9*, 299-309.
Ezratty, E.J., Bertaux, C., Marcantonio, E.E., and Gundersen, G.G. (2009). Clathrin mediates integrin endocytosis for focal adhesion disassembly in migrating cells. The Journal of cell biology *187*, 733-747.
Ezratty, E.J., Partridge, M.A., and Gundersen, G.G. (2005). Microtubule-induced focal adhesion disassembly is mediated by dynamin and focal adhesion kinase. Nature cell biology *7*, 581-590.
Field, J.J., Kanakkanthara, A., and Miller, J.H. (2014). Microtubule-targeting agents are clinically successful due to both mitotic and interphase impairment of microtubule function. Bioorganic & medicinal chemistry *22*, 5050-5059.
Fischer, R.S., Gardel, M., Ma, X., Adelstein, R.S., and Waterman, C.M. (2009). Local cortical tension by myosin II guides 3D endothelial cell branching. Current biology : CB *19*, 260-265.
Florian, S., and Mitchison, T.J. (2016). Anti-Microtubule Drugs. Methods in molecular biology *1413*, 403-421.

Ganguly, A., Yang, H., and Cabral, F. (2013). Detection and quantification of microtubule detachment from centrosomes and spindle poles. Methods in cell biology *115*, 49-62.
Gardel, M.L., Schneider, I.C., Aratyn-Schaus, Y., and Waterman, C.M. (2010). Mechanical integration of actin and adhesion dynamics in cell migration. Annual review of cell and developmental biology *26*, 315-333.
Gee, H.Y., Zhang, F., Ashraf, S., Kohl, S., Sadowski, C.E., Vega-Warner, V., Zhou, W., Lovric, S., Fang, H., Nettleton, M.*, et al.* (2015). KANK deficiency leads to podocyte dysfunction and nephrotic syndrome. The Journal of clinical investigation *125*, 2375-2384.
Geiger, B., Spatz, J.P., and Bershadsky, A.D. (2009). Environmental sensing through focal adhesions. Nature reviews Molecular cell biology *10*, 21-33.
Geiger, B., and Yamada, K.M. (2011). Molecular architecture and function of matrix adhesions. Cold Spring Harbor perspectives in biology *3*.
Horton, E.R., Humphries, J.D., James, J., Jones, M.C., Askari, J.A., and Humphries, M.J. (2016). The integrin adhesome network at a glance. Journal of cell science *129*, 4159-4163.
Hu, S., Dasbiswas, K., Guo, Z., Tee, Y.H., Thiagarajan, V., Hersen, P., Chew, T.L., Safran, S.A., Zaidel-Bar, R., and Bershadsky, A.D. (2017). Long-range self-organization of cytoskeletal myosin II filament stacks. Nature cell biology *19*, 133-141.
Jiu, Y., Peranen, J., Schaible, N., Cheng, F., Eriksson, J.E., Krishnan, R., and Lappalainen, P. (2017). Vimentin intermediate filaments control actin stress fiber assembly through GEF-H1 and RhoA. Journal of cell science *130*, 892-902.
Jones, G.E., Zicha, D., Dunn, G.A., Blundell, M., and Thrasher, A. (2002). Restoration of podosomes and chemotaxis in Wiskott-Aldrich syndrome macrophages following induced expression of WASp. The international journal of biochemistry & cell biology *34*, 806-815.
Joo, E.E., and Yamada, K.M. (2014). MYPT1 regulates contractility and microtubule acetylation to modulate integrin adhesions and matrix assembly. Nature communications *5*, 3510.
Juanes, M.A., Bouguenina, H., Eskin, J.A., Jaiswal, R., Badache, A., and Goode, B.L. (2017). Adenomatous polyposis coli nucleates actin assembly to drive cell migration and microtubule-induced focal adhesion turnover. The Journal of cell biology.
Kakinuma, N., Roy, B.C., Zhu, Y., Wang, Y., and Kiyama, R. (2008). Kank regulates RhoA-dependent formation of actin stress fibers and cell migration via 14-3-3 in PI3K-Akt signaling. The Journal of cell biology *181*, 537-549.
Kaverina, I., Krylyshkina, O., Gimona, M., Beningo, K., Wang, Y.L., and Small, J.V. (2000). Enforced polarisation and locomotion of fibroblasts lacking microtubules. Current biology : CB *10*, 739-742.
Kaverina, I., Rottner, K., and Small, J.V. (1998). Targeting, capture, and stabilization of microtubules at early focal adhesions. The Journal of cell biology *142*, 181-190.
Kaverina, I., and Straube, A. (2011). Regulation of cell migration by dynamic microtubules. Seminars in cell & developmental biology *22*, 968-974.
Kedziora, K.M., Isogai, T., Jalink, K., and Innocenti, M. (2016). Invadosomes - shaping actin networks to follow mechanical cues. Frontiers in bioscience *21*, 1092-1117.

Kopp, P., Lammers, R., Aepfelbacher, M., Woehlke, G., Rudel, T., Machuy, N., Steffen, W., and Linder, S. (2006). The kinesin KIF1C and microtubule plus ends regulate podosome dynamics in macrophages. Molecular biology of the cell *17*, 2811-2823.
Krendel, M., Zenke, F.T., and Bokoch, G.M. (2002). Nucleotide exchange factor GEF-H1 mediates cross-talk between microtubules and the actin cytoskeleton. Nature cell biology *4*, 294-301.
Krylyshkina, O., Kaverina, I., Kranewitter, W., Steffen, W., Alonso, M.C., Cross, R.A., and Small, J.V. (2002). Modulation of substrate adhesion dynamics via microtubule targeting requires kinesin-1. The Journal of cell biology *156*, 349-359.
Kwan, K.M., and Kirschner, M.W. (2005). A microtubule-binding Rho-GEF controls cell morphology during convergent extension of Xenopus laevis. Development *132*, 4599-4610.
Labernadie, A., Bouissou, A., Delobelle, P., Balor, S., Voituriez, R., Proag, A., Fourquaux, I., Thibault, C., Vieu, C., Poincloux, R.*, et al.* (2014). Protrusion force microscopy reveals oscillatory force generation and mechanosensing activity of human macrophage podosomes. Nature communications *5*, 5343.
Lansbergen, G., Grigoriev, I., Mimori-Kiyosue, Y., Ohtsuka, T., Higa, S., Kitajima, I., Demmers, J., Galjart, N., Houtsmuller, A.B., Grosveld, F.*, et al.* (2006). CLASPs attach microtubule plus ends to the cell cortex through a complex with LL5beta. Developmental cell *11*, 21-32.
Linder, S., Hufner, K., Wintergerst, U., and Aepfelbacher, M. (2000). Microtubule-dependent formation of podosomal adhesion structures in primary human macrophages. Journal of cell science *113 Pt 23*, 4165-4176.
Linder, S., Wiesner, C., and Himmel, M. (2011). Degrading devices: invadosomes in proteolytic cell invasion. Annual review of cell and developmental biology *27*, 185-211.
Lovelace, M.D., Powter, E.E., Coleman, P.R., Zhao, Y., Parker, A., Chang, G.H., Lay, A.J., Hunter, J., McGrath, A.P., Jormakka, M.*, et al.* (2017). The RhoGAP protein ARHGAP18/SENEX localizes to microtubules and regulates their stability in endothelial cells. Molecular biology of the cell *28*, 1066-1078.
Meddens, M.B., Pandzic, E., Slotman, J.A., Guillet, D., Joosten, B., Mennens, S., Paardekooper, L.M., Houtsmuller, A.B., van den Dries, K., Wiseman, P.W.*, et al.* (2016). Actomyosin-dependent dynamic spatial patterns of cytoskeletal components drive mesoscale podosome organization. Nature communications *7*, 13127.
Meiri, D., Marshall, C.B., Mokady, D., LaRose, J., Mullin, M., Gingras, A.C., Ikura, M., and Rottapel, R. (2014). Mechanistic insight into GPCR-mediated activation of the microtubule-associated RhoA exchange factor GEF-H1. Nature communications *5*, 4857.
Mortazavi, A., Williams, B.A., McCue, K., Schaeffer, L., and Wold, B. (2008). Mapping and quantifying mammalian transcriptomes by RNA-Seq. Nature methods *5*, 621-628.
Murphy, D.A., and Courtneidge, S.A. (2011). The 'ins' and 'outs' of podosomes and invadopodia: characteristics, formation and function. Nature reviews Molecular cell biology *12*, 413-426.

Oakes, P.W., Beckham, Y., Stricker, J., and Gardel, M.L. (2012). Tension is required but not sufficient for focal adhesion maturation without a stress fiber template. The Journal of cell biology *196*, 363-374.
Oakes, P.W., and Gardel, M.L. (2014). Stressing the limits of focal adhesion mechanosensitivity. Curr Opin Cell Biol *30*, 68-73.
Pan, C.Q., Liou, Y.-c., and Low, B.C. (2010). Active Mek2 as a regulatory scaffold that promotes Pin1 binding to BPGAP1 to suppress BPGAP1-induced acute Erk activation and cell migration. Journal of cell science *123*, 903-916.
Rafiq, N.B., Lieu, Z.Z., Jiang, T., Yu, C.H., Matsudaira, P., Jones, G.E., and Bershadsky, A.D. (2017). Podosome assembly is controlled by the GTPase ARF1 and its nucleotide exchange factor ARNO. The Journal of cell biology *216*, 181-197.
Ren, Y., Li, R., Zheng, Y., and Busch, H. (1998). Cloning and characterization of GEF-H1, a microtubule-associated guanine nucleotide exchange factor for Rac and Rho GTPases. The Journal of biological chemistry *273*, 34954-34960.
Rid, R., Schiefermeier, N., Grigoriev, I., Small, J.V., and Kaverina, I. (2005). The last but not the least: the origin and significance of trailing adhesions in fibroblastic cells. Cell motility and the cytoskeleton *61*, 161-171.
Riveline, D., Zamir, E., Balaban, N.Q., Schwarz, U.S., Ishizaki, T., Narumiya, S., Kam, Z., Geiger, B., and Bershadsky, A.D. (2001). Focal contacts as mechanosensors: externally applied local mechanical force induces growth of focal contacts by an mDia1-dependent and ROCK-independent mechanism. The Journal of cell biology *153*, 1175-1186.
Rodionov, V.I., Gyoeva, F.K., Tanaka, E., Bershadsky, A.D., Vasiliev, J.M., and Gelfand, V.I. (1993). Microtubule-dependent control of cell shape and pseudopodial activity is inhibited by the antibody to kinesin motor domain. The Journal of cell biology *123*, 1811-1820.
Sabass, B., Gardel, M.L., Waterman, C.M., and Schwarz, U.S. (2008). High resolution traction force microscopy based on experimental and computational advances. Biophysical journal *94*, 207-220.
Schachtner, H., Calaminus, S.D., Thomas, S.G., and Machesky, L.M. (2013). Podosomes in adhesion, migration, mechanosensing and matrix remodeling. Cytoskeleton *70*, 572-589.
Small, J.V., Geiger, B., Kaverina, I., and Bershadsky, A. (2002). How do microtubules guide migrating cells? Nature reviews Molecular cell biology *3*, 957-964.
Stehbens, S., and Wittmann, T. (2012). Targeting and transport: how microtubules control focal adhesion dynamics. The Journal of cell biology *198*, 481-489.
Stehbens, S.J., Paszek, M., Pemble, H., Ettinger, A., Gierke, S., and Wittmann, T. (2014). CLASPs link focal-adhesion-associated microtubule capture to localized exocytosis and adhesion site turnover. Nature cell biology *16*, 561-573.
Sun, Z., Tseng, H.Y., Tan, S., Senger, F., Kurzawa, L., Dedden, D., Mizuno, N., Wasik, A.A., Thery, M., Dunn, A.R.*, et al.* (2016). Kank2 activates talin, reduces force transduction across integrins and induces central adhesion formation. Nature cell biology *18*, 941-953.
Tee, Y.H., Shemesh, T., Thiagarajan, V., Hariadi, R.F., Anderson, K.L., Page, C., Volkmann, N., Hanein, D., Sivaramakrishnan, S., Kozlov, M.M.*, et al.* (2015). Cellular

chirality arising from the self-organization of the actin cytoskeleton. Nature cell biology *17*, 445-457.
van der Vaart, B., van Riel, W.E., Doodhi, H., Kevenaar, J.T., Katrukha, E.A., Gumy, L., Bouchet, B.P., Grigoriev, I., Spangler, S.A., Yu, K.L.*, et al.* (2013). CFEOM1-associated kinesin KIF21A is a cortical microtubule growth inhibitor. Developmental cell *27*, 145-160.
Vicente-Manzanares, M., and Horwitz, A.R. (2011). Adhesion dynamics at a glance. Journal of cell science *124*, 3923-3927.
Vicente-Manzanares, M., Ma, X., Adelstein, R.S., and Horwitz, A.R. (2009). Non-muscle myosin II takes centre stage in cell adhesion and migration. Nature reviews Molecular cell biology *10*, 778-790.
Vicente-Manzanares, M., Zareno, J., Whitmore, L., Choi, C.K., and Horwitz, A.F. (2007). Regulation of protrusion, adhesion dynamics, and polarity by myosins IIA and IIB in migrating cells. The Journal of cell biology *176*, 573-580.
Wittmann, T., and Waterman-Storer, C.M. (2001). Cell motility: can Rho GTPases and microtubules point the way? Journal of cell science *114*, 3795-3803.
Wu, X., Kodama, A., and Fuchs, E. (2008). ACF7 regulates cytoskeletal-focal adhesion dynamics and migration and has ATPase activity. Cell *135*, 137-148.
York, A.G., Chandris, P., Nogare, D.D., Head, J., Wawrzusin, P., Fischer, R.S., Chitnis, A., and Shroff, H. (2013). Instant super-resolution imaging in live cells and embryos via analog image processing. Nature methods *10*, 1122-1126.
Zaidel-Bar, R., Itzkovitz, S., Ma'ayan, A., Iyengar, R., and Geiger, B. (2007). Functional atlas of the integrin adhesome. Nature cell biology *9*, 858-867.
Zaidel-Bar, R., Zhenhuan, G., and Luxenburg, C. (2015). The contractome--a systems view of actomyosin contractility in non-muscle cells. Journal of cell science *128*, 2209-2217.
Zenke, F.T., Krendel, M., DerMardirossian, C., King, C.C., Bohl, B.P., and Bokoch, G.M. (2004). p21-activated kinase 1 phosphorylates and regulates 14-3-3 binding to GEF-H1, a microtubule-localized Rho exchange factor. The Journal of biological chemistry *279*, 18392-18400.
Zhang, Z., Nishimura, Y., and Kanchanawong, P. (2017). Extracting microtubule networks from superresolution single-molecule localization microscopy data. Molecular biology of the cell *28*, 333-345.
Zhu, X., Efimova, N., Arnette, C., Hanks, S.K., and Kaverina, I. (2016). Podosome dynamics and location in vascular smooth muscle cells require CLASP-dependent microtubule bending. Cytoskeleton *73*, 300-315.

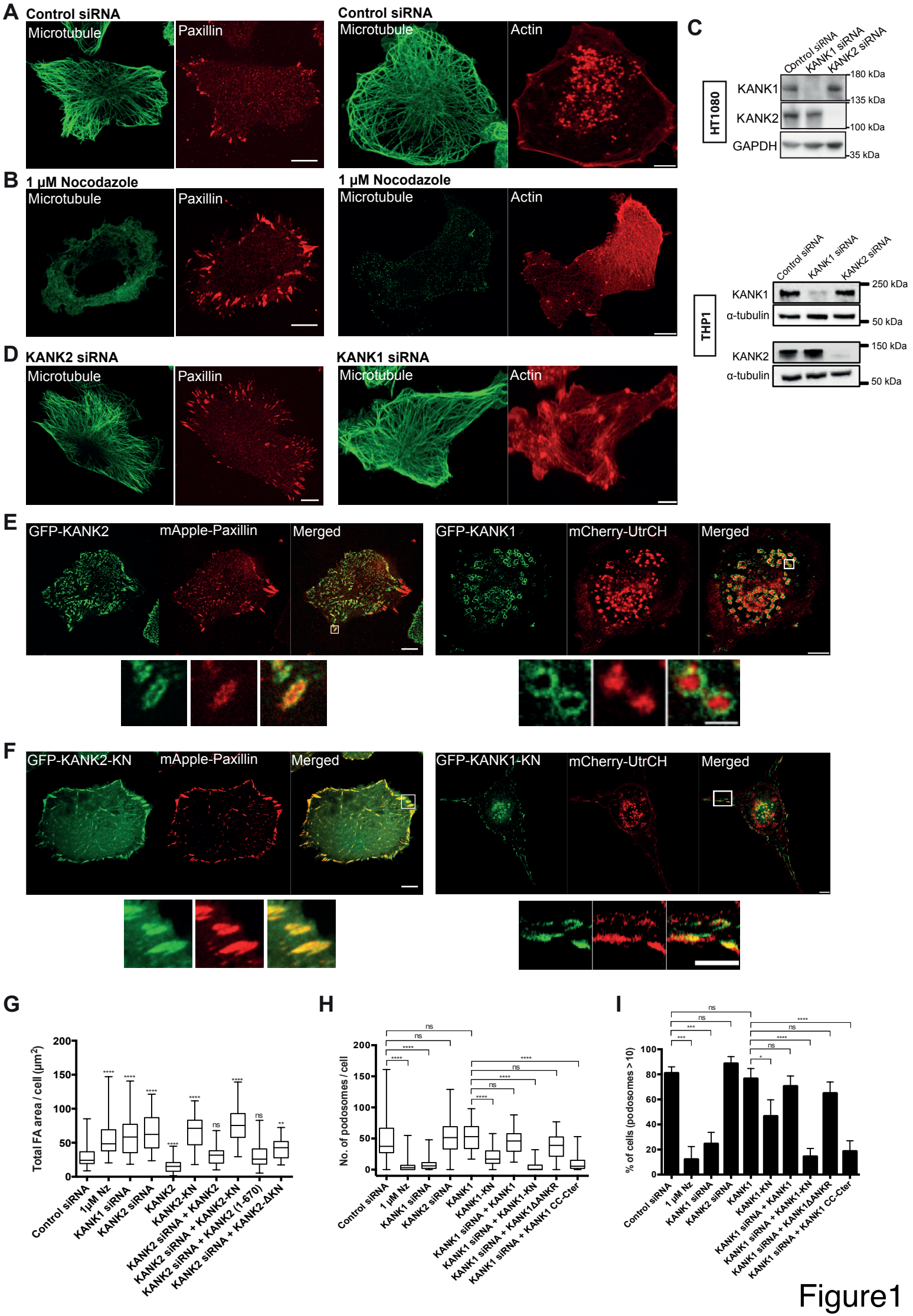
A
Control siRNA
Microtubule
Paxillin
Control siRNA
Microtubule
Actin
B
1 μM Nocodazole
Microtubule
Paxillin
1 μM Nocodazole
Microtubule
Actin
C
Control siRNA
KANK1 siRNA
KANK2 siRNA
HT1080
KANK1
KANK2
GAPDH
180 kDa
135 kDa
100 kDa
35 kDa
THP1
KANK1
α-tubulin
250 kDa
50 kDa
KANK2
α-tubulin
150 kDa
50 kDa
D
KANK2 siRNA
Microtubule
Paxillin
KANK1 siRNA
Microtubule
Actin
E
GFP-KANK2
mApple-Paxillin
Merged
GFP-KANK1
mCherry-UtrCH
Merged
F
GFP-KANK2-KN
mApple-Paxillin
Merged
GFP-KANK1-KN
mCherry-UtrCH
Merged
G
Total FA area / cell (μm²)
Control siRNA
1μM Nz
KANK1 siRNA
KANK2 siRNA
KANK2
KANK2-KN
KANK2 siRNA + KANK2
KANK2 siRNA + KANK2-KN
KANK2 siRNA + KANK2 (1-670)
KANK2 siRNA + KANK2-ΔKN
H
No. of podosomes / cell
Control siRNA
1 μM Nz
KANK1 siRNA
KANK2 siRNA
KANK1
KANK1-KN
KANK1 siRNA + KANK1
KANK1 siRNA + KANK1-KN
KANK1 siRNA + KANK1ΔANKR
KANK1 siRNA + KANK1 CC-Cter
I
% of cells (podosomes > 10)
Control siRNA
1 μM Nz
KANK1 siRNA
KANK2 siRNA
KANK1
KANK1-KN
KANK1 siRNA + KANK1
KANK1 siRNA + KANK1-KN
KANK1 siRNA + KANK1ΔANKR
KANK1 siRNA + KANK1 CC-Cter

Figure1

Figure 2

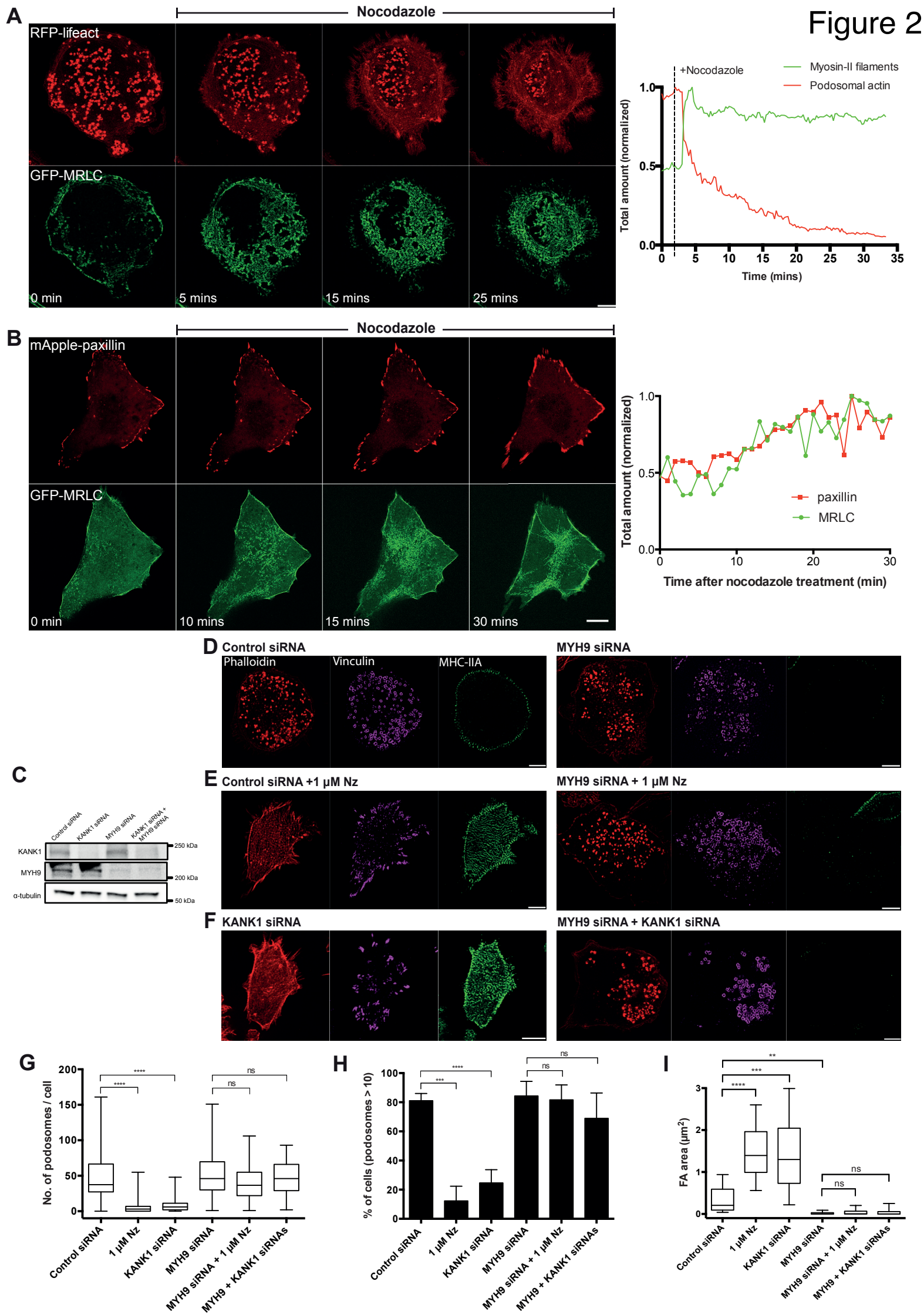
A
Nocodazole
RFP-lifeact
GFP-MRLC
0 min
5 mins
15 mins
25 mins
+Nocodazole
Myosin-II filaments
Podosomal actin
Total amount (normalized)
Time (mins)
B
Nocodazole
mApple-paxillin
GFP-MRLC
0 min
10 mins
15 mins
30 mins
paxillin
MRLC
Total amount (normalized)
Time after nocodazole treatment (min)
C
Control siRNA
KANK1 siRNA
MYH9 siRNA
KANK1 siRNA + MYH9 siRNA
KANK1
MYH9
α-tubulin
250 kDa
200 kDa
50 kDa
D
Control siRNA
Phalloidin
Vinculin
MHC-IIA
MYH9 siRNA
E
Control siRNA +1 μM Nz
MYH9 siRNA + 1 μM Nz
F
KANK1 siRNA
MYH9 siRNA + KANK1 siRNA
G
No. of podosomes / cell
H
% of cells (podosomes > 10)
I
FA area (μm²)
Control siRNA
1 μM Nz
KANK1 siRNA
MYH9 siRNA
MYH9 siRNA + 1 μM Nz
MYH9 + KANK1 siRNAs

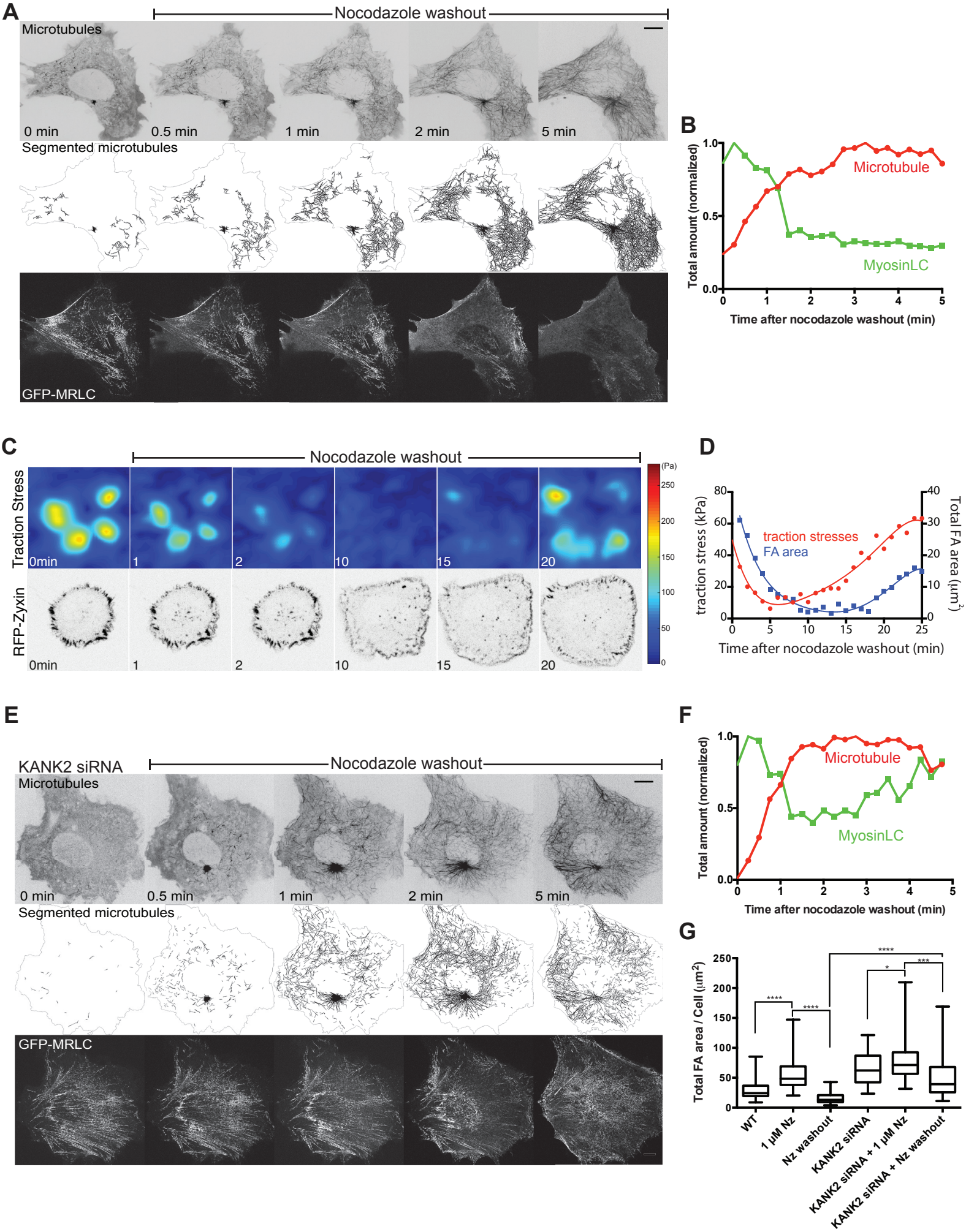
A
Nocodazole washout
Microtubules
0 min
0.5 min
1 min
2 min
5 min
Segmented microtubules
GFP-MRLC
B
Microtubule
MyosinLC
Total amount (normalized)
Time after nocodazole washout (min)
C
Nocodazole washout
Traction Stress
RFP-Zyxin
0min
1
2
10
15
20
(Pa)
D
traction stresses
FA area
traction stress (kPa)
Total FA area (μm²)
Time after nocodazole washout (min)
E
KANK2 siRNA
Nocodazole washout
Microtubules
0 min
0.5 min
1 min
2 min
5 min
Segmented microtubules
GFP-MRLC
F
Microtubule
MyosinLC
Total amount (normalized)
Time after nocodazole washout (min)
G
Total FA area / Cell (μm²)
WT
1 μM Nz
Nz washout
KANK2 siRNA
KANK2 siRNA + 1 μM Nz
KANK2 siRNA + Nz washout

Figure 3

Figure 4

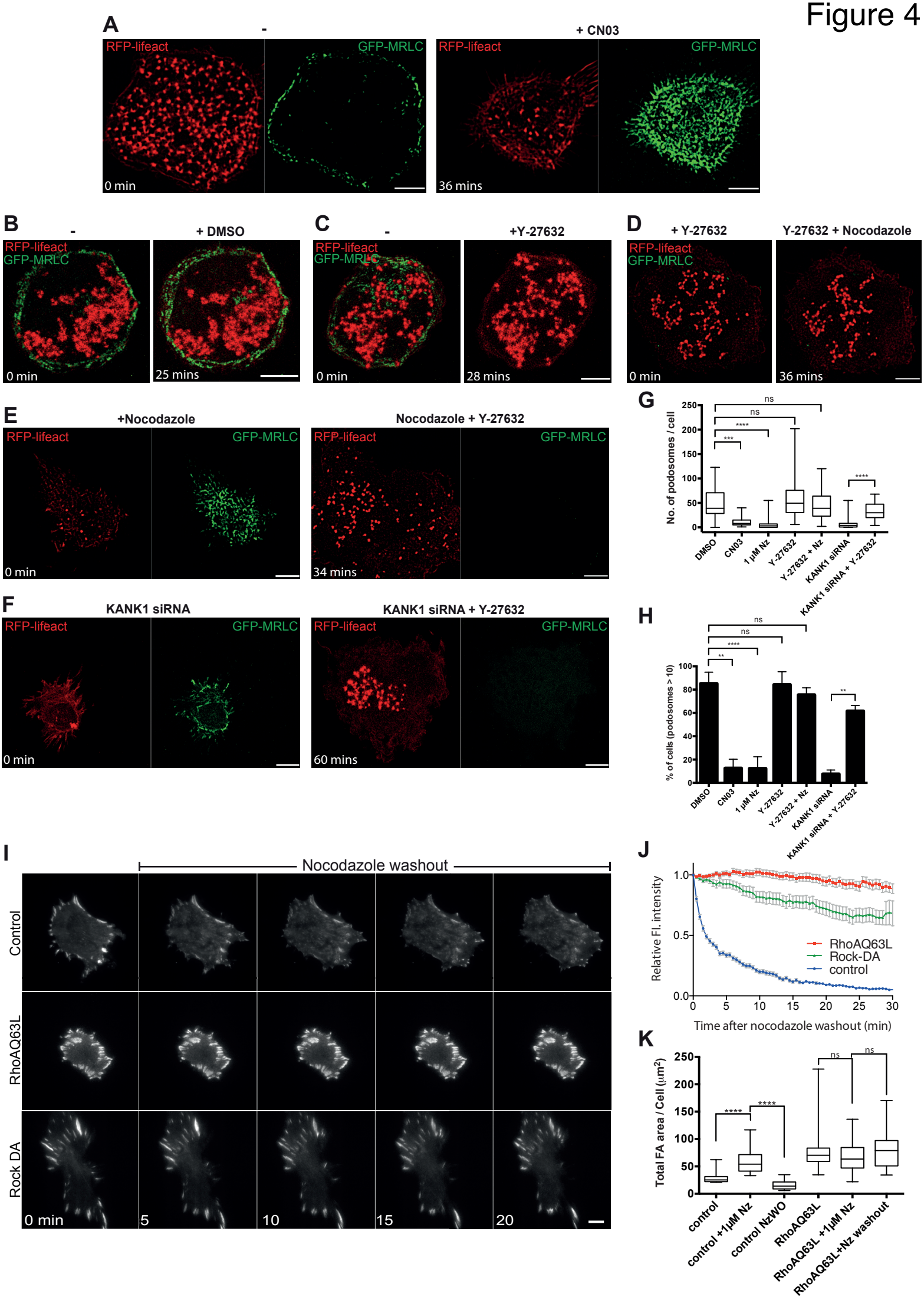
A
-
+ CN03
RFP-lifeact
GFP-MRLC
0 min
36 mins
B
-
+ DMSO
25 mins
C
+Y-27632
28 mins
D
+ Y-27632
Y-27632 + Nocodazole
36 mins
E
+Nocodazole
Nocodazole + Y-27632
34 mins
F
KANK1 siRNA
KANK1 siRNA + Y-27632
60 mins
G
No. of podosomes / cell
DMSO
CN03
1 μM Nz
Y-27632
Y-27632 + Nz
KANK1 siRNA
KANK1 siRNA + Y-27632
ns
****
***
H
% of cells (podosomes > 10)
**
I
Nocodazole washout
Control
RhoAQ63L
Rock DA
5
10
15
20
J
Relative Fl. intensity
RhoAQ63L
Rock-DA
control
Time after nocodazole washout (min)
K
Total FA area / Cell (μm²)
control
control +1μM Nz
control NzWO
RhoAQ63L
RhoAQ63L +1μM Nz
RhoAQ63L+Nz washout

Figure 5

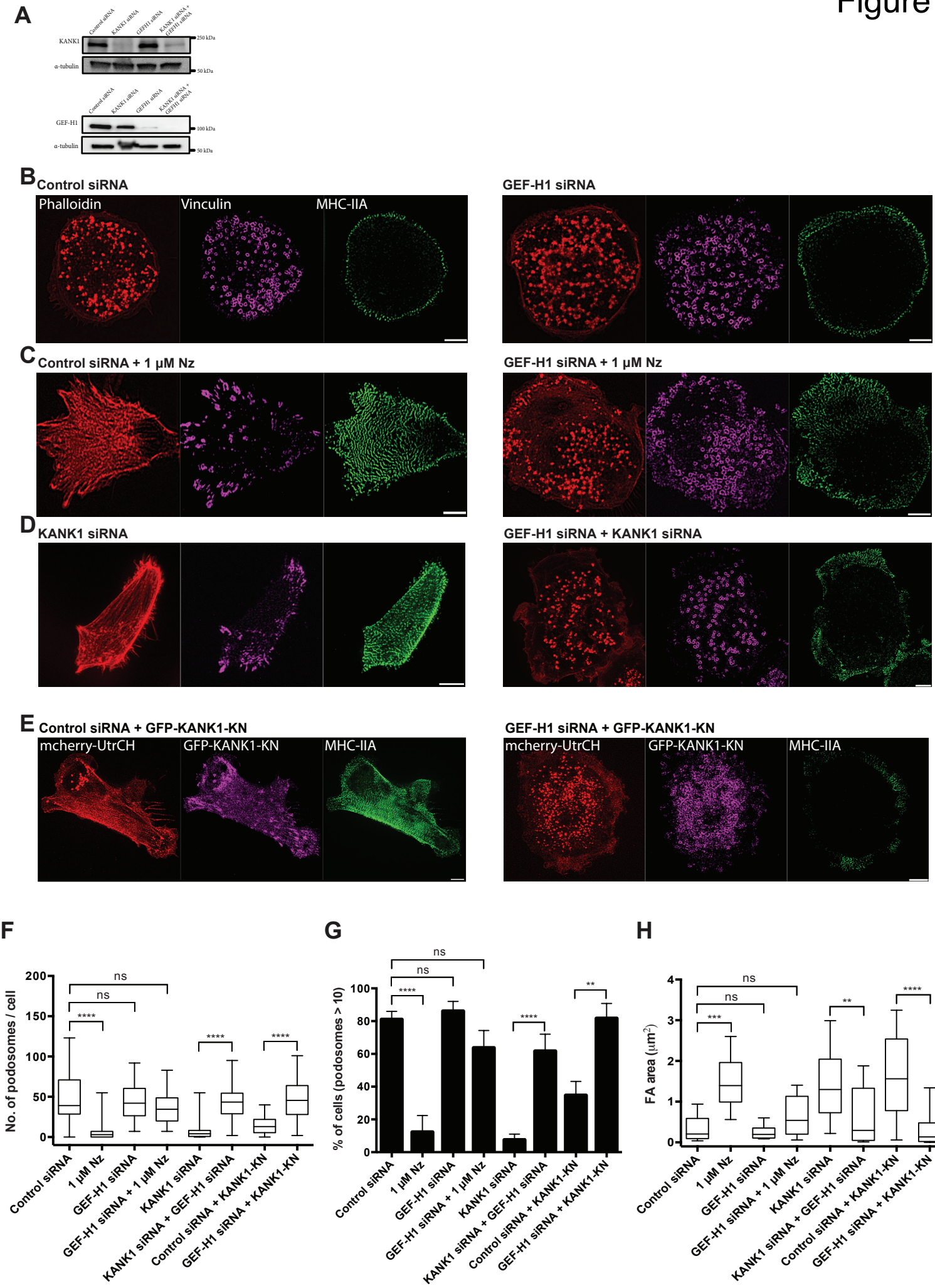
A
Control siRNA
KANK1 siRNA
GEF-H1 siRNA
KANK1 siRNA + GEF-H1 siRNA
KANK1
α-tubulin
250 kDa
50 kDa
GEF-H1
100 kDa
B
Control siRNA
GEF-H1 siRNA
Phalloidin
Vinculin
MHC-IIA
C
Control siRNA + 1 μM Nz
GEF-H1 siRNA + 1 μM Nz
D
KANK1 siRNA
GEF-H1 siRNA + KANK1 siRNA
E
Control siRNA + GFP-KANK1-KN
GEF-H1 siRNA + GFP-KANK1-KN
mcherry-UtrCH
GFP-KANK1-KN
MHC-IIA
F
No. of podosomes / cell
G
% of cells (podosomes > 10)
H
FA area (μm²)
ns
****
***
**
Control siRNA
1 μM Nz
GEF-H1 siRNA
GEF-H1 siRNA + 1 μM Nz
KANK1 siRNA
KANK1 siRNA + GEF-H1 siRNA
Control siRNA + KANK1-KN
GEF-H1 siRNA + KANK1-KN

Figure 6

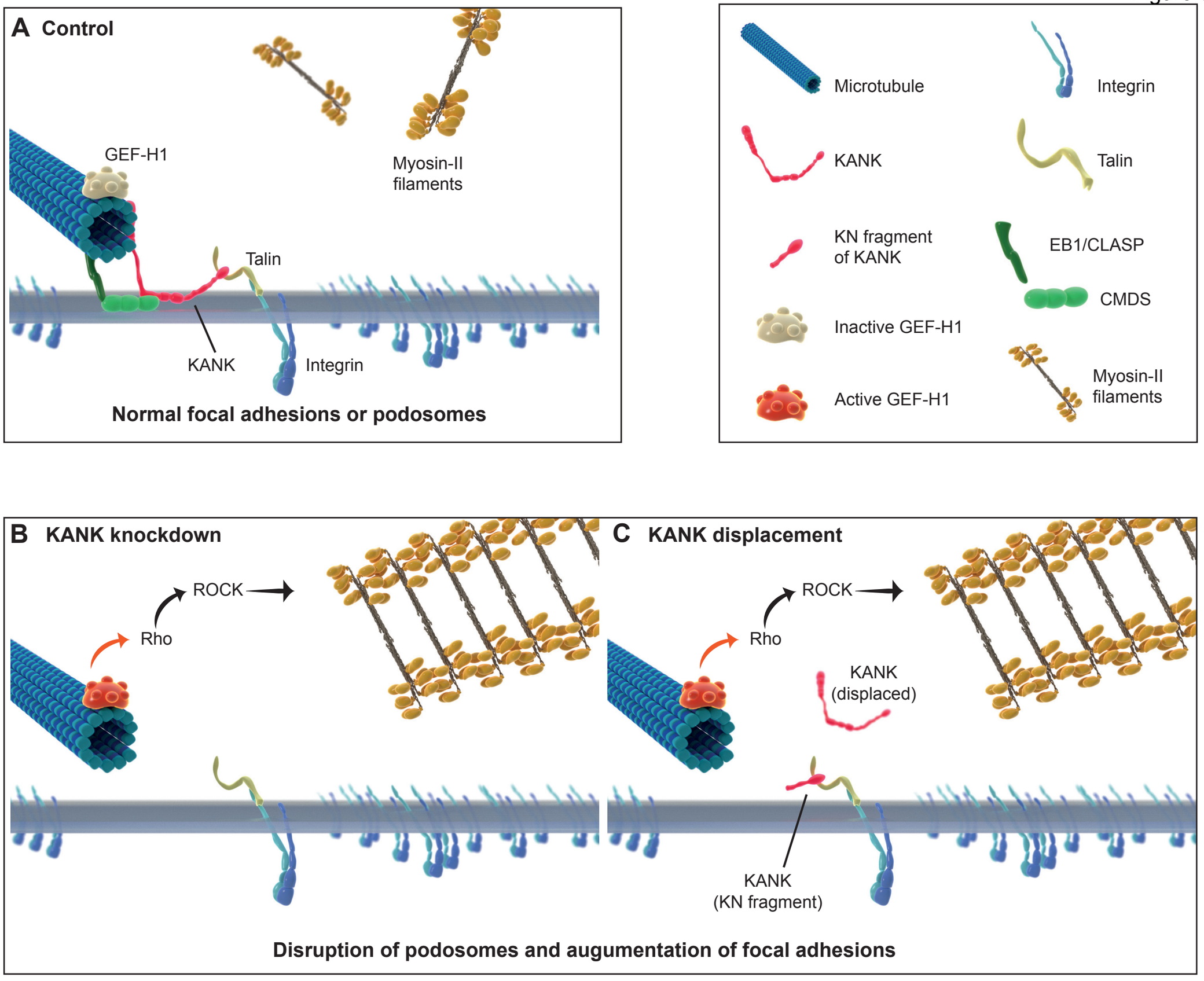
A Control
GEF-H1
Myosin-II filaments
Talin
KANK
Integrin
Normal focal adhesions or podosomes
Microtubule
Integrin
KANK
Talin
KN fragment of KANK
EB1/CLASP
CMDS
Inactive GEF-H1
Active GEF-H1
Myosin-II filaments
B KANK knockdown
ROCK
Rho
C KANK displacement
ROCK
Rho
KANK (displaced)
KANK (KN fragment)
Disruption of podosomes and augumentation of focal adhesions